Effective RhB Dye Removal Using Sustainable Natural Bioadsorbents Synthesized from Avocado Seed and Skin

Sayra Orozco · **Esteban Montiel** · **Jaime Espino Valencia** ·
Roberto Guerra González · **María del Carmen Chávez Parga** ·
José Apolinar Cortés · **Michel Rivero**

Abstract Managing waste generated by the food industry is a pressing environmental challenge, and traditional disposal methods such as landfilling or incineration are no longer viable solutions. However, by recovering and valorizing waste in wastewater treatment, we can address the waste management issue and the energy-intensive nature of conventional treatment methods with processes compatible with renewable energy technologies. In this work, avocado skin and seed are valorized for their application in removing Rhodamine B (RhB) dye. Avocado skin (ASk) and seed (ASe) were recovered and recycled separately to develop natural bioadsorbents. Biomaterials were characterized by XRD, XPS, ICP-MS, ATR-FTIR spectroscopy, TGA, N_2 adsorption/desorption, and SEM. The ASk and ASe bioadsorbents were employed to remove RhB at four experimental conditions: pH, RhB concentration, bioadsorbent concentration, and temperature. RhB removal was followed by UV–Vis spectroscopy. The results show that at pH 3, the highest percentages of dye removal are achieved, using ASk and ASe, with 88 and 92% removal, respectively. ASe bioadsorbent is more effective for removing RhB dye, reaching 92% after 4 h of contact with 2 g L^{-1} of bioadsorbent and at 30 °C. Experimental results better fit a pseudo-second-order kinetic model and the Langmuir adsorption model, with maximum adsorption capacities of 13.1240 and 17.9998 mg g^{-1} for ASk and ASe, respectively. The results show that natural bioadsorbents are suitable options for environmental remediation.

S. Orozco · J. E. Valencia · M. del Carmen Chávez Parga · J. A. Cortés
Posgrado de Ingeniería Química, Universidad Michoacana de San Nicolás de Hidalgo, Ciudad Universitaria, 58060 Morelia, Michoacan, Mexico
e-mail: sorozcocerros@gmail.com

E. Montiel
Escuela de Estudios Superiores de Xalostoc, Universidad Autónoma del Estado de Morelos, 62715 Xalostoc, Morelos, Mexico

R. G. González
Facultad de Ingeniería Química, Universidad Michoacana de San Nicolás de Hidalgo, Ciudad Universitaria, 58060 Morelia, Michoacan, Mexico

M. Rivero (✉)
Instituto de Investigaciones en Materiales, Unidad Morelia, Universidad Nacional Autónoma de México, Col. Ex Hacienda de San José de La Huerta Morelia, 58190 Antigua Carretera a Pátzcuaro No. 8701, Michoacan, Mexico
e-mail: mrivero@materiales.unam.mx

⚙ Springer

1 Introduction

Avocado *Persea americana* is a typical Mexican fruit with exceptional nutritional properties. In 2022, the global avocado market reached 14.85 billion dollars and is estimated to grow at an annual rate of 7.2% from 2023 to 2030 (GVR-4–68,039-929–5., 2022). Mexico is the largest avocado producer in the world with 2393 thousand metric tons (Shahbandeh, 2022), with the largest production center in Michoacan, in central Mexico (Denvir, 2023; Gómez-Tagle et al., 2022). Avocado is considered a superfood due to its nutritional properties (Zafar & Sidhu, 2011). It has also been processed to develop new products such as guacamole, frozen slices, sauces, puree, dehydrated, and avocado oil to satisfy consumers' needs and incorporate them into new eating styles.

In avocado processing, seeds and skin are considered waste by-products and thus discarded. According to Rodríguez-Martínez et al. (2022), around 2 million tons of seeds and skin were generated worldwide in 2019. Mostly, these by-products still need to be recovered and valorized; otherwise, they will develop serious pollution problems due to inadequate management. These are generally discharged into aquifers or open dumps, causing soil and groundwater contamination. In the framework of the General Law of Circular Economy in Mexico (de Difusión y Publicaciones, 2021), the valorization of these wastes is essential, as it would bring strategies for waste management and economic and environmental benefits (Bitonto et al., 2021; Duque-Acevedo et al., 2020; Tesfaye et al., 2022; Venugopal, 2022). The avocado seed and skin represent a significant percentage of the avocado fruit (13–17%, or 311–406 thousand metric tons just in Mexico). They contain macromolecules such as polysaccharides, proteins, lipids, minerals, and vitamins (Bangar et al., 2022; Permal et al., 2023; Rashama et al., 2022; Restrepo-Serna et al., 2022; Rodríguez-Martínez et al., 2022) that can be further exploited. The by-products of processed avocado can be used for energy generation (Rashama et al., 2022; San José et al., 2023; Sangaré et al., 2022), development of bioproducts such as biofuels, oils, snacks, pharmaceuticals (Bitonto et al., 2021; Permal et al., 2023; Piedrahita-Rodríguez et al., 2023; Rashama et al., 2022), biomaterials (Ahmad & Danish, 2022; Asiagwu et al., 2013, 2017; Bazzo et al., 2015; Boeykens et al., 2018; Elizalde González et al., 2007; Ibrahim et al., 2023; Leite et al., 2017; Mallampati et al., 2015), among others (see Fig. 1).

Biomaterials derived from biomass waste constitute a feasible economic-environmental alternative for their valorization (Balbay & Acıkgoz, 2022). Due to their composition, these biomaterials own many functional groups, which facilitates their use as bio-adsorbents. Thus, they have gained increasing attention in recent years for removing recalcitrant organic pollutants present in water (Adegoke & Bello, 2015; Souza et al., 2020; Xing et al., 2008), such as anthracene (Enahoro Agarry, 2016), phenolic compounds (Leite et al., 2017), acetaminophen (Villaescusa et al., 2011), and heavy metals such as Ni (Gupta & Jain, 2021; Mallampati et al., 2015), Cu (Ligas et al., 2022; Pereira et al., 2021), Cd (Bahsaine et al., 2023), Pb, Cr (Boeykens et al., 2018, 2019; Foroutan et al., 2019; Gupta & Jain, 2021; Ligas et al., 2022; Mahmoud et al., 2022; Mallampati et al., 2015), Hg (Yu et al., 2016), among others. Untreated wastewater containing hazardous substances poses significant risks to public health and disrupts aquatic ecosystems. Moreover, producing everyday items such as textiles, rubber, plastics, leather, cosmetics, and paper contaminates water streams. An example is the textile industry, which has water-intensive practices such as bleaching, dyeing, and printing. In particular, dyeing can cause visual pollution and introduces bioaccumulative dyes that may form unwanted hazardous
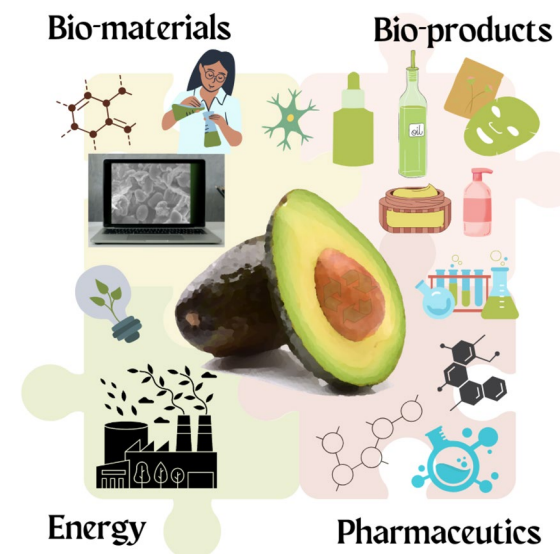

Fig. 1 Uses of avocado seeds and skin

byproducts when metabolized by microorganisms. Various dyes are used in industry, including natural and synthetic, among which we can find rhodamine B (RhB). RhB has been associated with environmental concerns due to its potential toxicity and persistence in water systems. This article discusses RhB dye as a contaminant in wastewater and explores effective and sustainable methods for removing it from wastewater streams.

The bioadsorption process for organic compounds is highly efficient and simple, and does not produce degradation intermediates (Enahoro Agarry, 2016). The most common bioadsorbents consist of biomaterials activated by different chemical and thermal processes (Aichour et al., 2018; Al-Gheethi et al., 2022; Arivoli et al., 2009; Bahsaine et al., 2023; Berrazoum et al., 2015; Besegatto et al., 2021; Cheng et al., 2017; Elizalde González et al., 2007; Kasiri, 2019; Leite et al., 2017; Lima et al., 2020; Z. Liu et al., 2022; Sahu & Singh, 2019; Yadav et al., 2022). The surface functionalization of activated carbon leads to high adsorption capacity, surface area, and reactivity. Nevertheless, its synthesis from waste biomass and its regeneration needs energy-intensive thermal and chemical processes, which conveys a big challenge for up-scaling to the industrial level. Therefore, materials that can easily integrate sustainable energy solutions, such as solar power, should be developed. In this regard, natural biomaterials are emerging as an alternative to activated carbon. The simple and low-cost synthesis processes of natural biomaterials make it possible to use low-temperature solar systems for drying biomass waste. Solar drying is a sustainable energy supply in the agro-industry (Ortiz-Rodríguez et al., 2022) and reduces the overall carbon footprint of the derived material. Literature reported the development of natural bioadsorbents from several sources, such as banana (Boeykens et al., 2018; Enahoro Agarry, 2016), mandarin (Besegatto et al., 2021), avocado skin (Boeykens et al., 2018) and seed (Asiagwu et al., 2017; Bazzo et al., 2015; Mahmoud et al., 2022), cashew leaf and carnauba straw (Pereira et al., 2021), peanut shell (Boeykens et al., 2018), olive (Albanio et al., 2021), sugarcane bagasse (Boeykens et al., 2018), and others (Rahim et al., 2021; Rashid et al., 2021).

Natural bioadsorbents from avocado waste have been used to remove anionic and cationic dyes, demonstrating high efficacy (Asiagwu et al., 2013;

Bazzo et al., 2015; Mallampati et al., 2015; Netto et al., 2019). Bioadsorbents from avocado seeds have been extensively researched in literature, but only a few studies explore the potential of avocado skin as biosorbents, let alone compare their adsorption capabilities.

This work reports the valorization of avocado seed and skin for developing low-cost bioadsorbent materials. These natural bioadsorbents are applied to remove a model dye (RhB) under different experimental conditions: pH, RhB concentration, bioadsorbent concentration, and temperature. Other bioadsorbents from waste-activated bioadsorbents have been used for RhB removal (Al-Gheethi et al., 2022; Arivoli et al., 2009; Z. Liu et al., 2022). However, the study of removing this dye with natural bioadsorbents from avocado residues has not been reported.

2 Methodology

2.1 Materials

Rhodamine B ($C_{28}H_{31}ClN_2O_3$, 99.9%) was used as the pollutant model, and KCl to control the ionic strength. pH adjustment was done with nitric acid (HNO_3, 60–66% conc.) and potassium hydroxide (KOH, 85%). All chemicals were purchased from Merck as A.C.S reagent grade and used as received without further purification.

2.2 Recovery and Valorized

Avocado skin (ASk) and seed (ASe) were harvested and washed to remove pulp excess and minimize microorganisms' growth. Once washed, seed and skin were cut into pieces of approximately 1×1 cm, followed by a drying process in an oven at 50 °C for 72 h and grinding in an electric mill. Then, the pulverized biomaterials were sieved using a 410-μm mesh. These biomaterials were characterized and evaluated as bioadsorbents for RhB dye removal. Note that a low-temperature methodology was used to synthesize the bioadsorbents, which avoids using chemical precursors for activation, aiming for a green chemistry approach. Moreover, considering dehydration is the most energy-consuming process; it is feasible to substitute it with solar drying systems assisted with

suitable phase change materials and conventional means to ensure a continuous sustainable process.

2.3 Characterization

To determine moisture and composition of volatile, organic, and inorganic matter of ASk and ASe bioadsorbents, a thermogravimetric method was applied according to Norma Mexicana (NMX-AA-034-SCFI-2015), detailed in Section A in the SM.

The leaching of minerals on the ASk and ASe bioadsorbents in acidic conditions (pH 3) was determined by inductively coupled plasma mass spectrometry, ICP-MS (iCAP Qc Model, Thermo Scientific). The samples were prepared by adding 0.2 g of the bioadsorbents to 100 mL of water at pH 3. The supernatant was collected after centrifugation at 7500 rpm and analyzed by ICP-MS.

The ASk and ASe bioadsorbents were characterized by thermogravimetric analysis (TGA), Fourier transform infrared (FTIR) spectroscopy, X-ray diffraction (XRD), X-ray photoelectron spectroscopy (XPS), inductively coupled plasma mass spectrometry (ICP-MS), N_2 adsorption–desorption isotherm, and scanning electron microscopy (SEM).

The crystalline structure of the materials was analyzed with a Bruker D2-Phaser diffractometer using CuKα radiation at 30 kV and 10 mA. Diffractograms were scanned at 2θ angles from 5 to 80° with 0.5 s per step and increments of 0.0100806°.

X-ray photoelectron spectroscopy (XPS) analyses were carried out in an ultra-high vacuum (UHV) system scanning XPS microprobe PHI 5000 VersaProbe II, with an Al Kα X-ray source $h\nu = 1486.6$ eV) monochromatic with 100-µm beam diameter, and a multi-channel detector (MCD) analyzer. The XPS spectra were obtained at 45° to the normal surface, pressure 5×10^{-7} Pa, constant analyzing energy (CAE) $E_0 = 117.40$, 11.75 eV survey surface, and high-resolution narrow scan. The surface samples were not etched. The peak positions were referenced to the background Ag $3d_{5/2}$ photopeak at 368.20 eV, with an FWHM of 0.81 eV, and C$1s$ hydrocarbon groups at 285.00 eV, Au $4f_{7/2}$ at 84.00 eV central peak core level position. The XPS spectrum was fitted with the MultiPak PHI software and Spectral Data Processor, SDP v 4.1.

The specific surface area and average pore diameter of ASk and ASe bioadsorbents were determined by adsorption/desorption isotherms using liquid N_2 (77 K) obtained in a Gemini 3240 Micromeritics BET Surface Analyzer and its degassing unit. The bioadsorbents samples were first degassed at 100 °C for 24 h under vacuum conditions of 2.5 mbar to eliminate moisture before adsorption measurements. The specific surface area of bioadsorbents was estimated by the BET (Brunauer–Emmett–Teller) methodology.

The bioadsorbents morphology was observed with a JEOL (model JSM-7600F) microscope, equipped with an Oxford brand EDS detector (model INCA X-Act).

The attenuated total reflectance Fourier transform infrared (ATR-FTIR) spectroscopy allowed us to identify the functional groups on the bioadsorbents. ATR-FTIR spectra were collected using a Thermo Scientific Nicolet iS10 FTIR spectrometer fitted with a Thermo Scientific Smart iTR™ ATR accessory with a diamond crystal and using the OMNIC software. Powder samples were added directly onto the crystal for analysis at room temperature without applying pressure. Sixteen spectra were obtained and coadded for each sample covering a range of 4000–650 cm^{-1} at a spectral resolution of 4 cm^{-1}. A background spectrum was obtained by collecting a similar number of scans after cleaning the diamond crystal with acetone.

Thermogravimetric analysis was obtained using a Perkin Elmer thermal analyzer Model STA 6000, using oxygen gas at 30 cm min^{-1}, 20 mg of material, and heating from 25 to 850 °C at 10 °C min^{-1}.

The pH value at the isoelectric point (IEP) was determined according to the method described by Aichour et al. (2018), Bello et al. (2015), and Inyinbor et al. (2015). This method is based on the pH change recorded after reaching the chemical equilibrium while controlling the ionic strength with a 0.1 M KCl solution. For this analysis, we considered pH values of 2, 4, 6, 8, and 10 and a concentration of the bioadsorbent of 2 g L^{-1}. The procedure is as follows: a given volume of a 0.1 M aqueous KCl solution is prepared, and the initial pH (pH$_i$) is adjusted to a given value (using 0.1 NaOH or 0.1 M HCl). The solution is brought in contact with the bioadsorbent ASk or ASe and kept in agitation for 48 h at room temperature. After the time has elapsed, the final pH value (pH$_f$) is measured and recorded. This procedure is repeated for all considered pH values. Then, the pH value at the IEP is obtained graphically when plotting

the pH change $\Delta pH = pH_f\text{-}pH_i$ as a function of the pH. The pH value at the IEP corresponds to the zero intersection of the curve.

2.4 Analytic Methods

The UV–Vis absorbance spectrum of RhB at different pH was measured with a Hach DR6000 spectrophotometer to observe the chemical stability of RhB. Fig. S1 in the supplementary material shows these spectra, at pH 1.91, 3.02, 4.01, 6.01, and 11.61. The RhB dye has different absorbance peaks in the UV–Vis region for a 12 mg L^{-1} concentration. The absorption bands correspond to the main functional groups of the dye molecule (see Fig. S1 in the SM): the chromophore group containing the structure amino (NH^+) absorbs in the visible region in 0.556 µm at pH 1.91, 3.02, and 4.01, and in 0.554 µm at pH 6.01 and 11.61. The chromophore group shift is attributed to the charge separation, in which the carboxylate anion (R^-) takes a proton at acid pH, resulting in (R^+), which accepts the same resonant structures and therefore exhibits a similar absorption spectrum with a shift in the chromophore group.

The removal process of RhB was evaluated from its characteristic absorption peak at 0.556 µm (pH 3) and 0.554 µm (pH 5, 7, and 9). Absorption spectra of the samples in the wavelength range 0.2–0.7 µm were measured with a spectrophotometer Evolution 300 Thermo Scientific, with a spectral interval of 0.004 µm. pH measurements were conducted with a HANNA pH meter, calibrated with standard buffer solutions of 3.01 ± 0.02 and 7.01 ± 0.02 (25 °C).

2.5 Bioadsorption Capacity Test

The adsorption tests of ASk and ASe bioadsorbents were studied by RhB dye removal. Experiments were carried out in a system with hydrodynamic batch operation and constant stirring to obtain a homogeneous adsorbent suspension, controlling temperature to a defined value. The adsorption process efficiency relies on several factors. In this work, the evaluated factors are the adsorbent concentration (0.5, 1, 2, 3 g L^{-1}), adsorbate concentration (6, 12, 24, 36, 48, 60, and 72 mg L^{-1}), pH (3, 5, 7, and 9), and temperature (30, 40, 50, 60, and 70 °C).

The experimental procedure is as follows. The synthetic colored solution was prepared by dissolving the required amount of RhB (0.6, 1.2, 2.4, 3.6, 4.8, 6.0, and 7.2 mg) in 0.1 L of deionized water to get the desired concentration. The initial pH of the solution was adjusted to 3, 5, 7, or 9 through a nitric acid solution (1% vol.) or potassium hydroxide (1% weight). At this time ($t = t_0$), the first sample was taken. Then 0.5, 1, 2, or 3 g L^{-1} of ASk or ASe bioadsorbents was added to the synthetic-colored solution under constant stirring. The adsorption process was carried out for 240 min to reach the adsorption/desorption equilibrium. Samples were taken at 15, 30, 60, 120, 180, and 240 min. For each sample, the bioadsorbent was separated by centrifugation at 7500 rpm for 2 min to analyze the evolution of the RhB dye concentration by UV–Vis spectroscopy. All experiments were performed in triplicate.

3 Results

3.1 Characterization

3.1.1 Composition

The adsorption behavior of biomaterials depends on their chemical composition, and such effects must be evaluated to avoid drawing incorrect conclusions about the process. Table 1 shows the composition of ASk and ASe bioadsorbents. The ASe bioadsorbent possesses higher moisture content than ASk, which can be attributed to the ASe's higher adsorption capacity of water molecules. The volatile matter content (hemicellulose, cellulose, and lignin) is similar for both samples. The ASk bioadsorbent has a higher fixed carbon value and ash content than the ASe bioadsorbent. The authors (Rotta et al., 2016) reported an ash content of $5.43 \pm 0.49\%$, consistent with the

Table 1 ASk and ASe bioadsorbent composition

Bioadsorbent	Moisture [%]	Volatile matter [%]	Fixed carbon [%]	Ash [%]
ASk	24.67 ± 0.18	66.81 ± 0.37	3.60 ± 0.21	4.89 ± 0.02
ASe	31.77 ± 0.19	67.20 ± 0.25	0.74 ± 0.06	0.28 ± 0.01

results of this work, related to the minerals present in avocado skin. These compositions offer the possibility of employing this residue for food products.

The leaching of the minerals on the ASk and ASe bioadsorbents under acidic conditions (pH 3) was determined by ICP-MS. The mineral content is shown in Table 2. The results show higher P, K, Ca, and Zn leaching for the ASk bioadsorbent concerning ASe. This can be attributed to the higher mineral content in avocado skin than in seeds, corroborating results presented in Table 1.
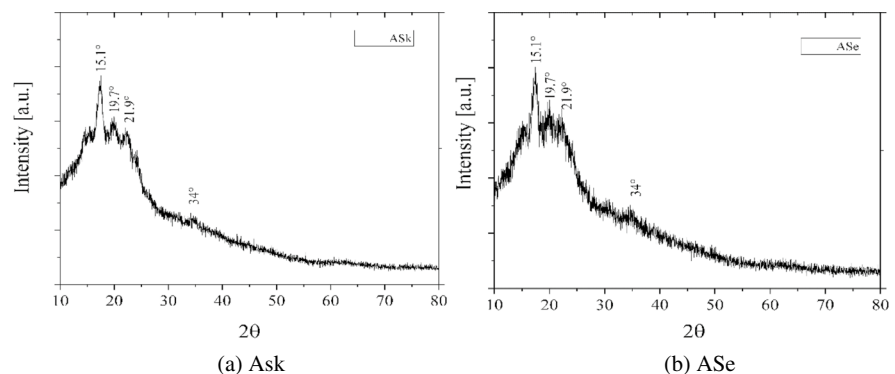
3.1.2 X-ray Diffraction

XRD patterns for ASk and ASe bioadsorbents are shown in Fig. 2. The diffraction peaks in the XRD pattern of ASk and ASe are consistent with those reported in the literature (Pereira et al., 2021), with a peak at $2\theta = 15.1°$ characteristic of cellulose I, according to JCPDS 00–056-1718 (Ishikawa et al., 2015). For both materials, a low-intensity peak at $2\theta = 21.9°$ is observed, associated with a cellulose crystalline region (Pereira et al., 2021). For residual biomass resources, the degree of crystallinity depends on the sample's composition. For example, Pereira et al. (2021) report that materials composed of lignin, cellulose, and hemicellulose have a low crystallinity. This agrees with our results, where we observed that both materials have undefined broad peaks.

3.1.3 X-ray Photoelectron Spectroscopy

Figures 3 and 4 present the X-ray photoelectron spectroscopy results for ASk and ASe bioadsorbents, respectively. These spectra show peaks centered at 285, 400, and 532 eV, corresponding to C1s, N1s, and O1s, respectively. Nevertheless, the peak associated with the N-containing functional group is low due to the low nitrogen content in both biomaterials.

To identify the functional groups containing oxygen and carbon in the ASk and ASe bioadsorbents, the major O1s and C1s peaks were deconvoluted, see Figs. 3 and 4. The C1s peak was deconvoluted into four individual curves from the groups listed in Table 3, where the relative content of each component is presented for both bioadsorbents: C=C present in lignin at 284.35 to 248.46 eV; C–C in cellulose and hemicellulose at 284.94–285.15 eV; CO in hydroxyl, phenol, or ether groups at 285.92–286.17 eV; C=O in carbonyl, ester, or carboxyl groups at 287.20–287.30 eV; and π-π^* transitions in the aromatic carbon at 288.56–288.88 eV (Araújo et al., 2023; Lan et al., 2019; Q.-X. Liu et al., 2019). These C-containing functional groups are present in hemicellulose, cellulose, and lignin polymers, corroborating XRD results (see Fig. 2).

In turn, the O1s peak was deconvoluted into three individual curves (see Figs. 3b and 4b) from the groups listed in Table 4 and its relative contents of

Table 2 ASk and ASe bioadsorbents composition. The relative standard deviation is indicated in parentheses

ND not detected

Bioadsorbent	Mg [mg L^{-1}]	P [mg L^{-1}]	K [mg L^{-1}]	Ca [mg L^{-1}]	Fe [mg L^{-1}]	Zn [mg L^{-1}]
ASk	2.2983(4.4)	8.3564(2.4)	143.402(0.6)	0.8011(9.2)	ND(–)	0.94(2.1)
ASe	3.3345(0.7)	3.4739(0.9)	39.3946(0.6)	0.16701(1.2)	0.0091(2.1)	0.2841(0.8)

Fig. 2 XRD patterns of **a** ASk and **b** ASe bioadsorbents

(a) Ask

(b) ASe

Fig. 3 XPS spectra of ASk bioadsorbent

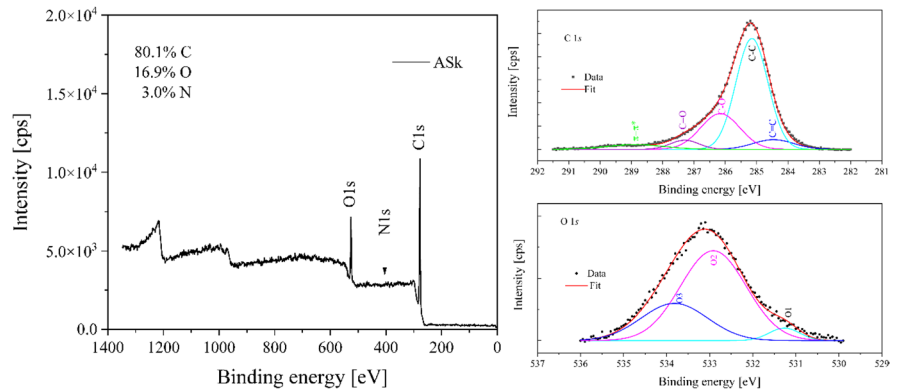**Fig. 4** XPS spectra of ASe bioadsorbent
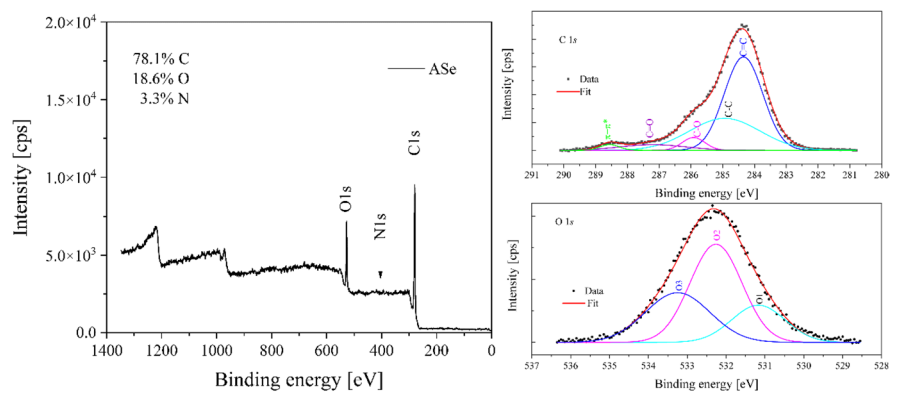
Table 3 Deconvolution results of C1s spectra of ASk and ASe bioadsorbents

Functional group	ASk			ASe		
	Position eV	FWHM eV	Relative content [%]	Position eV	FWHM eV	Relative content [%]
C=C	284.46	1.52	6.7	284.35	1.43	54.3
C–C	285.15	1.20	60.3	284.94	2.61	34.0
C–O	286.17	1.47	23.9	285.92	0.85	4.4
C=O	287.30	1.07	4.4	287.20	2.44	5.6
π-π*	288.88	2.16	4.7	288.56	0.71	1.7

Table 4 Deconvolution results of O1s spectra of ASk and ASe bioadsorbents

Functional group	ASk			ASe		
	Position eV	FWHM eV	Relative content [%]	Position eV	FWHM eV	Relative content [%]
C=O	531.27	0.84	4.4	531.17	1.62	19.3
C–O	532.92	1.80	67.4	532.26	1.57	49.5
C–OH	533.82	1.81	28.2	533.25	1.96	31.2

each component present in ASk and ASe bioadsorbents. O1 at 531.17–531.27 eV is assigned to C=O binding, O2 at 532.26–532.92 eV corresponds to C–O binding, and O3 at 533.25–533.82 eV to C–OH (Araújo et al., 2023; Lan et al., 2019). The ASk and ASe bioadsorbents have O-containing functional groups on their surface, which are effective adsorption sites.

The deconvolution data shows that the ASk bioadsorbent contains mainly hemicellulose and cellulose (C–C, C–O, C–OH groups in higher proportion), and in lower proportion lignin (C=C and C=O groups). In contrast, the ASe bioadsorbent has a higher proportion of C=C groups, corresponding to lignin.

3.1.4 FT-IR Spectroscopy

The FT-IR spectra of the bioadsorbents ASk and ASe are shown in Fig. 5. Since both materials have a similar composition, their corresponding spectra are alike. In the FT-IR spectra, the broadband around 3280 cm^{-1} corresponds to the stretching vibration of the H–O–H band. The band observed between 3000 and 2820 cm^{-1} is attributed to asymmetric and symmetric C–H sp^3 stretching of alkane compounds (Berrazoum et al., 2015; Enahoro Agarry, 2016; Mokhtari et al., 2021). A weak signal at 1726 cm^{-1} is related to the C–O group stretching of the ester group (Inyinbor et al., 2015), while the band in the region of 1600 cm^{-1} due to the C=O stretching vibrations of carbonyl structure (Berrazoum et al., 2015; Besegatto et al., 2021). The band between 1200 and 1059 cm^{-1}
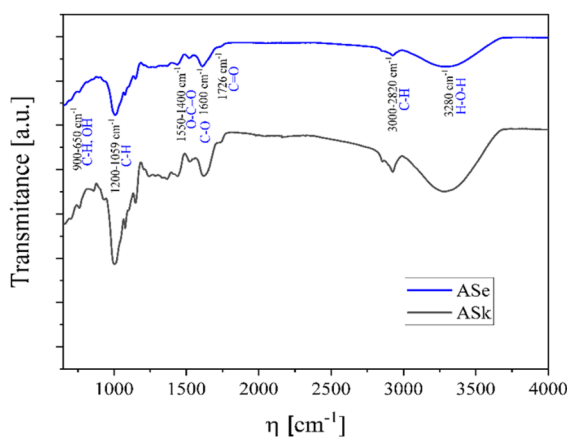
corresponds to the vibrations of the C–OH group, present in alcohols (Cheng et al., 2017; Pereira et al., 2021). All these functional groups are present in the cellulose structure. In the region from 900 to 650 cm^{-1}, some bands associated with the out-of-plane bending mode of C–H or O–H groups are present (Cheng et al., 2017). Finally, at 900 cm^{-1}, we observe a characteristic peak of glycosidic linkages in cellulose (Mokhtari et al., 2021; Netto et al., 2019). The functional groups identified by IR spectroscopy are consistent with those identified by XPS (see Figs. 3 and 4), which correspond to hemicellulose, cellulose, and lignin polymers.

3.1.5 Thermogravimetric Analysis

TGA analysis of ASk and ASe bioadsorbents was carried out under an oxygen atmosphere during the whole characterization, from ambient temperature up to 850°C. This analysis allowed the evaluation of the biosorbents' stability.

Figure 6 shows the weight percentage loss and weight derivative as a function of the sample temperature for ASk and ASe bioadsorbents. As observed, both bioadsorbents exhibit similar thermal behavior. The main composition of the ASk and ASe bioadsorbents are hemicellulose, cellulose, and, to a lesser extent, lignin, lipids, and fats (see Table 1, and minerals in Table 2) (Paniagua et al., 2021), consistent with XPS and FT-IR results (see Figs. 3, 4, and 5, respectively). The weight loss process is mainly due to the decomposition of hemicellulose and cellulose, considered volatile matter. In literature, the decomposition ranges are reported as hemicellulose at 190–320°C, cellulose at 280–400°C, and lignin at 320–450°C (Paniagua et al., 2021).

3.1.6 N$_2$ Adsorption/Desorption

The BET surface areas of ASk and ASe bioadsorbents were determined in the range 0.05–0.30 P/P$_0$, where the linearity of the BET equation is satisfied. The determined values of the BET areas are 0.4249 and 0.6112 m^2 g^{-1} for ASk and ASe, while their corresponding total pore volumes are 0.0014 and 0.0016 cm^3 g^{-1}, respectively. Natural bioadsorbents have a low area surface compared to other synthesized activated biomass. This is due to the low synthesis temperatures (50 to 100°C), where the

Fig. 5 FT-IR spectra of ASk and ASe bioadsorbents

Fig. 6 Weight loss and weight derivative as a function of the sample temperature for **a** ASk and **b** ASe bioadsorbents

(a) Skin

(b) Seed
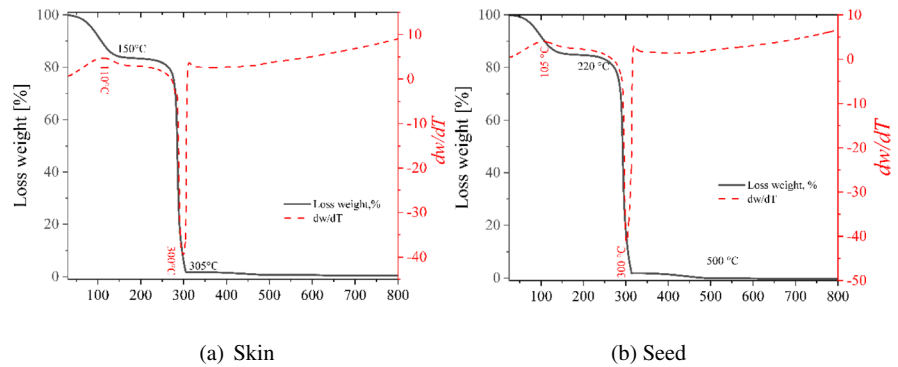
biomass carbonation does not occur. BET surface area and total pore volume values for natural bioadsorbents from avocado seed have been reported in the literature as 2.16 m^2 g^{-1} and 0.0105 cm^3 g^{-1} in Netto et al. (2019), and 1.75 m^2 g^{-1} and 0.0039 cm^3 g^{-1} in Bazzo et al. (2015), respectively, while Boeykens et al. (2019) reported values from 0.0813 to 0.1276 m^2 g^{-1} and 0.0001 cm^3 g^{-1}, which are of the order to those determined in this work. According to the moisture content analysis, see Table 1, the ASe bioadsorbent has a higher capacity to adsorb water molecules related to its higher surface area when compared to the ASk bioadsorbent.

It is important to note that structural and morphological modification of the materials can increase the surface area at the cost of increased energy or chemical consumption. However, this does not guarantee a greater capacity for adsorption since other factors influence the process.

3.1.7 Microscopy

Figure 7 shows the micrographs of the fresh bioadsorbents recovered and valorized from avocado skin and seed. Their microstructures are disordered matrices in which polysaccharide spheres, in the order of 2 μm for ASk and 16 μm for ASe, are bound together. The morphology of both bioadsorbents is typical of natural bioadsorbents (untreated) and agrees with those reported by Bazzo et al. (2015), Netto et al. (2019), and Sangaré et al. (2022). We can observe cracks on both materials. However, pores are not visible, which is consistent with the obtained low total pore volume (0.0014 and 0.0016 cm^3 g^{-1} for ASk and ASe bioadsorbents, respectively), and consequently, their corresponding low surface areas (0.4249 and 0.6112 m^2 g^{-1} for ASk and ASe) and characteristic of natural bioadsorbents (Pereira et al., 2021).

3.1.8 Isoelectric Point

Figure 8 shows the pH change ($\Delta pH = \Delta pH_f - \Delta pH_i$) as a function of pH, as

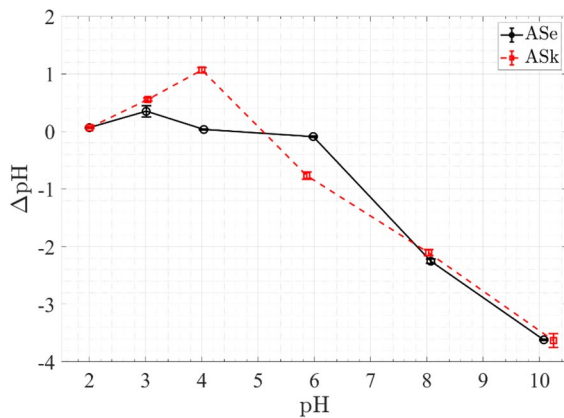**Fig. 7** Microscopy of **a** ASk and **b** Ase bioadsorbent

(a) Skin

(b) Seed
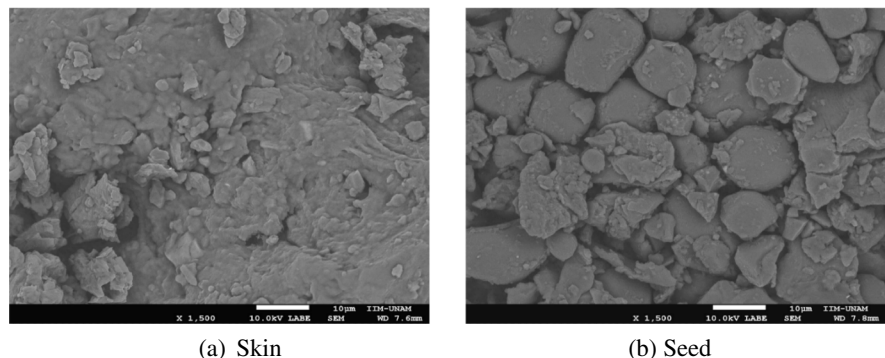
Fig. 8 pH isoelectric point for ASk and ASe bioadsorbents

Table 5 pH-IEP for bioadsorbents

Bioadsorbent	pH	Ref
ASk	5.09	This work
ASe	4.50	This work
Avocado seed	6.40	Bazzo et al. (2015)
Avocado seed	8.12	Netto et al. (2019)
Unripe plantain peel	6.0	Enahoro Agarry (2016)
Municipal solid waste	6.5	Berrazoum et al. (2015)
Waste carbon	7.2	Cheng et al. (2017)
Endocarps of *Irvingia gabonensis*	6.4–6.6	Inyinbor et al. (2015)
Activated lemon peels	3.8–8.1	Aichour et al. (2018)

described in Sect. 2.3. The intersection of the curve with $\Delta pH = 0$ corresponds to the pH value at the isoelectric point. The pH values at the isoelectric point are 5.09 and 4.50 for ASk and ASe, respectively. The behavior observed in Fig. 8 is consistent with that reported by Bazzo et al. (2015) for a natural bioadsorbent of the avocado seed. Table 5 presents the pH-IEP values for different natural or activated bioadsorbents.

For pH values below the IEP, the ASk or ASe adsorbents have a positive surface charge and act as an ion exchanger. Conversely, the surface charge of ASk or ASe adsorbents is negative at pH values above the corresponding IEP, which benefits the cation adsorption.

3.2 Dye Removal by Bioadsorption

Evaluating the bioadsorption capacity of ASk and ASe adsorbents requires determining the experimental conditions for pH, the concentrations of adsorbent and adsorbate, and temperature. The values of interest for these variables were selected according to those reported in the literature for rhodamine B adsorption (Inyinbor et al., 2015; Z. Liu et al., 2022). We achieved this by carrying out a set of experiments for each variable. The following results are discussed in terms of the dye removal percentage. Namely, we evaluate the dye RhB concentration change in time t (C_t) compared to the initial RhB concentration (C_0). This change is given by Eq. (1).

$$Removal, \% = \frac{C_0 - C_t}{C_0} \times 100 \tag{1}$$

To evaluate the influence of pH variation on the RhB structure during adsorption, solutions of RdB 12 mg L^{-1}) were prepared at pH values of 3, 5, 7, and 9 in absence of ASe and ASk adsorbents. The concentration of RhB was measured at 0, 60, 120, 180, and 240 min. The degradation profiles of RhB at indicated pH values are shown in Fig. S2 in the SM. These results show that pH does not significantly affect RhB concentration. Therefore, the RhB removal is attributed to the adsorption process under the conditions explored in the present work.

3.2.1 pH Effect

The pH value is relevant in adsorption processes because it modifies the adsorbent's surface charge and the adsorbate's ionization. Therefore, we first investigate the bioadsorbent's adsorption capacity under different pH values.

The removal of RhB dye with ASk and ASe bioadsorbents at pH 3, 5, 7, and 9 is presented in Fig. 9. For this purpose, we take the initial concentration of ASk or ASe bioadsorbent and adsorbate (RhB) within the reported ranges (Liu et al., 2022), namely 2 and 12 mg L^{-1}, respectively. The temperature of the adsorption process was 30 °C. As seen in Fig. 9, the removal percentage is inversely proportional to the pH value, namely, the higher removal was obtained at pH 3 for both biomaterials. The RhB removal after

Fig. 9 RhB removal profiles at different pH values for both bioadsorbents; 2 g L^{-1} of adsorbent, dye concentration 12 mg L^{-1}, 30 °C
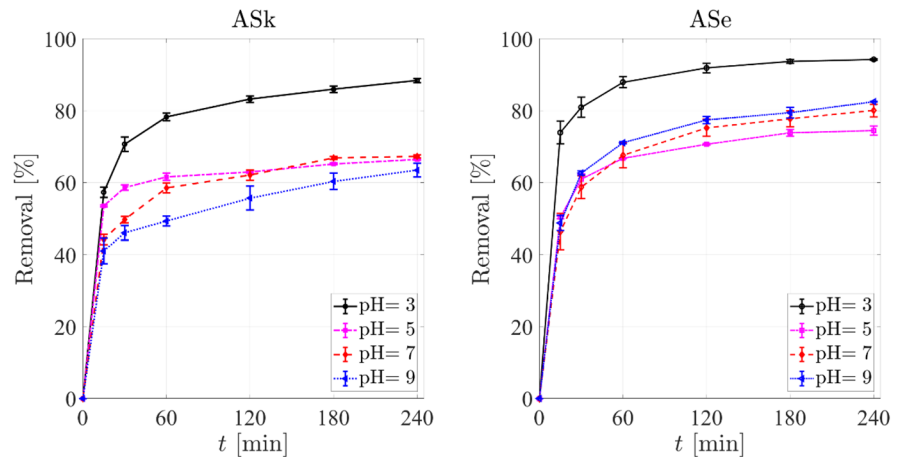
240 min at pH 3 is 88 and 94% for ASk and ASe, respectively. Note that for the ASk bioadsorbent at pH 5, 7, and 9, a similar removal is achieved (66, 67, and 63%, respectively) although, at early stages, more significant differences are observed. This is not the case for the bioadsorbent ASe, which exhibits a similar behavior for the pH values referenced, and whose differences lie within the experimental deviation.

The influence of the pH value on the removal of RhB dye may be related to the electrostatic interactions between the adsorbate and the bioadsorbent (Al-Gheethi et al., 2022). Namely, at a given pH, the electrostatic interactions between the partial surface charge of the bioadsorbents and the cationic or anionic behavior of RhB influence the adsorption mechanism. In Sect. 3.1.8, the pH value in the IEP was determined as 4.50 for ASe and 5.09 for ASk. Therefore, at pH 3, where the bioadsorption process is higher, ASk and ASe have a partially positive charged surface and zwitterions of RhB (pK$_a$ = 3.7) coexistence. Thus, the adsorption mechanism may result from (i) the HO-π interactions or hydrogen bonding between the functional groups –OH and –OOC of the ASk or ASe bioadsorbents (see Fig. 5) and zwitterions of rhodamine (Zimnitsky et al., 2006), or (ii) the electrostatic interaction between the positive surface charge of the bioadsorbent and the negatively charged carboxyl groups of the RhB molecule (Al-Gheethi et al., 2022; Bello et al., 2015; Inyinbor et al., 2015).

Our observations are consistent with results for RhB removal, in which the process reached the highest adsorbate removal values at pH 3, using other bioadsorbents from agricultural residues such as *Banyan*

aerial roots modified (Fan et al., 2020), *Raphia-Hookene* (88.88% removal) (Inyinbor et al., 2015), *Gmelina Abores* (91% removal) (Bello et al., 2015), *Argemone mexicana* (70% removal) (Khamparia & Jaspal, 2016), *Irvingia gabonesis* (78.6% removal) (Inyinbor et al., 2015), and *Moringa Oleifera* (94.76% removal) (Bello et al., 2015).

At pH above 5, the ASk and ASe bioadsorbents have a negative surface charge, and RhB has an anionic behavior, leading to an electrostatic repulsion between RhB molecules and the material. Therefore, the process can be attributed to hydrogen bonding with the hydroxyl groups of the bioadsorbents ASk and ASe (see Fig. 5) (Fan et al., 2020).

3.2.2 Adsorbent Concentration

The effect of the amount of ASk and ASe bioadsorbent was studied at four different concentrations: 0.5, 1, 2, and 3 g L^{-1}. The experimental conditions of the removal process were at pH 3, where the adsorption process achieved the highest removal percentage. In turn, we used an adsorbate (RhB dye) concentration of 12 mg L^{-1} at 30 °C.

The removal profiles of RhB dye using ASk and ASe bioadsorbents at the different adsorbent concentrations (0.5, 1, 2, and 3 g L^{-1}) are presented in Fig. 10. As shown, the percentage removal increases with the bioadsorbent concentration for both bioadsorbents. Other works obtained similar results (Al-Gheethi et al., 2022; Asiagwu et al., 2013; Enahoro Agarry, 2016). These results can be attributed to a higher bioadsorbent concentration,

Fig. 10 RhB removal profiles at different adsorbent concentrations for both biomaterials. pH 3, dye concentration 12 mg L^{-1}, 30 °C
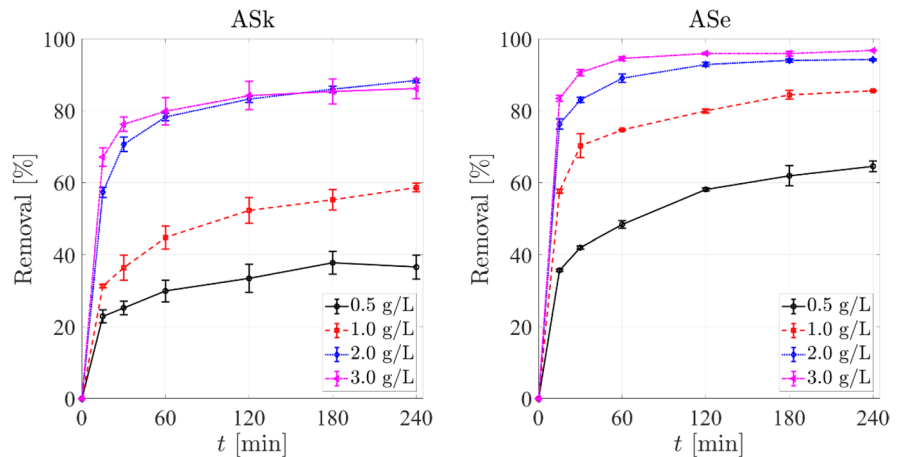
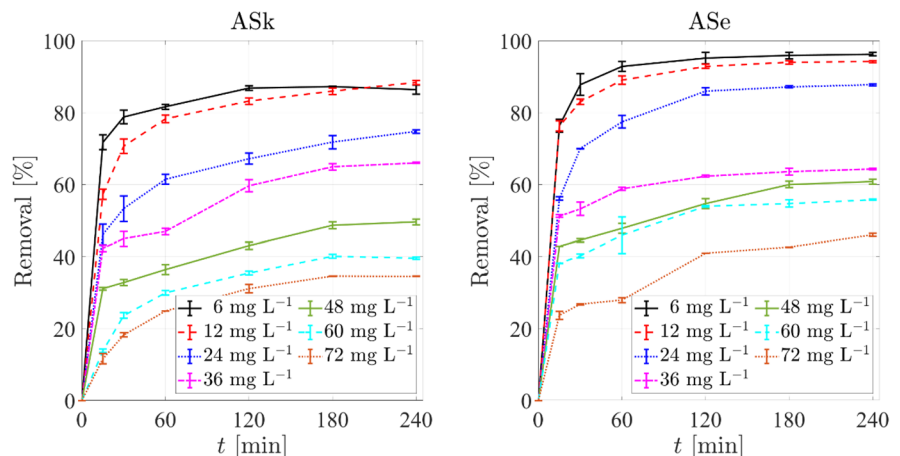increasing the available adsorption sites for the RhB dye to adsorb. Nevertheless, no significant enhancement is observed for 3 g L^{-1} of absorbent with respect to a concentration of 2 g L^{-1}. This indicates that the maximum adsorption capacity of these bioadsorbents has been reached, which is consistent with other reported values (Al-Gheethi et al., 2022; Enahoro Agarry, 2016). The saturation of the materials can be attributed to partial aggregation of the adsorbents, decreasing the number of available sites. Finally, it is noteworthy that ASe biomaterial outperforms the percentage removal of ASk for all adsorbent concentrations, which can be attributed to the larger surface area of the ASe (0.6112 m^2 g^{-1}) than that of the ASk bioadsorbent (0.4249 m^2 g^{-1}).

3.2.3 Initial RhB Dye Concentration

The effect of the initial RhB dye concentration on the adsorption process was investigated at seven different values: 6, 12, 24, 36, 48, 60, and 72 mg L^{-1}. The experimental conditions for the RhB dye removal process correspond to those obtained in the previous analyses: pH 3 and bioadsorbent concentration (for both ASk and ASe) of 2 g L^{-1}. As in previous cases, the adsorption process was carried out at 30 °C. The removal profiles for both bioadsorbents at the given RhB dye concentrations are presented in Fig. 11. As shown, the RhB dye removal percentage decreases with increasing adsorbate concentration, consistent with values reported in other works (Al-Gheethi et al., 2022; Asiagwu et al., 2013). This can be attributed to the fact that as the adsorbate concentration

Fig. 11 RhB removal profiles at different adsorbate concentrations for both biomaterials. pH 3, 2 g L^{-1} of adsorbent, 30 °C

(dye RhB) increases, more molecules compete for the available adsorption sites.

For the ASk bioadsorbent, the percentage removal (at a contact time of 240 min) is 86, 84, 75, 66, 50, 40, and 35% at 6, 12, 24, 36, 48, 60, and 72 mg L^{-1}, respectively. As for ASe, the corresponding percentages are 96, 94, 88, 64, 61, 56, and 46%, respectively. Namely, with ASe, a higher removal is obtained than with ASk.

3.2.4 Temperature Effect

Temperature is a parameter that influences the adsorption process, as it affects the activation energy (Wang et al., 2020). Thus, in this section, we investigate the effect of temperature on the adsorption capacity. Four different temperatures (40, 50, 60, and 70 °C) were tested and compared with those obtained at 30 °C. The temperature effect has been studied for three RhB concentrations (12, 24, and 48 mg L^{-1}), selected based on previous results. The experimental conditions were those used in the last case: a pH 3 and bioadsorbent (ASk and ASe) concentration of 2 g L^{-1}. The removal profiles of RhB dye using ASk and ASe bioadsorbents at different temperatures for 12, 24, and 48 mg L^{-1} RhB concentrations are presented in Figs. 12 and 13, respectively.

The RhB dye removal profiles for the ASk bioadsorbent (see Fig. 12) show a similar behavior: a slight enhancement in the adsorption process from 30 to 50 °C (being more pronounced with 12 and 48 mg

L^{-1} of adsorbate) followed by a larger drop at higher temperatures (more significant for 12 and 24 mg L^{-1}). This decrease can be attributed to a reduction in the surface activity by the degradation of the material occurring above 50 °C and acid conditions (pH 3). Aksu and Tezer (2000) reported a similar behavior in removing Remazol Black B dye with a *Rhizopus arrhizus* bioadsorbent. As for the ASe bioadsorbent (Fig. 13), the tendency described for ASk was observed just for an adsorbate concentration of 24 mg L^{-1}. For 12 and 48 mg L^{-1}, RhB concentrations exhibit a monotonous decrease in dye removal as the temperature increases for most of the adsorption process, being steeper the change from 50 to 70 °C (up to 40%).

The results for ASk, in which increasing temperature from 30 to 50 °C favors the absorption process, suggest an endothermic process. Conversely, for the ASe bioadsorbent, temperature increase does not favor absorption, suggesting an exothermic process. This will be elucidated by a thermodynamic analysis described in the next section.

3.3 Thermodynamic Analysis

Investigating the influence of temperature on the adsorption process requires determining the change in the thermodynamic parameters enthalpy (ΔH^0), Gibbs free energy (ΔG^0), and entropy (ΔS^0) for both bioadsorbents. These parameters are indicators of the possible nature of adsorption (Mokhtari et al., 2021)
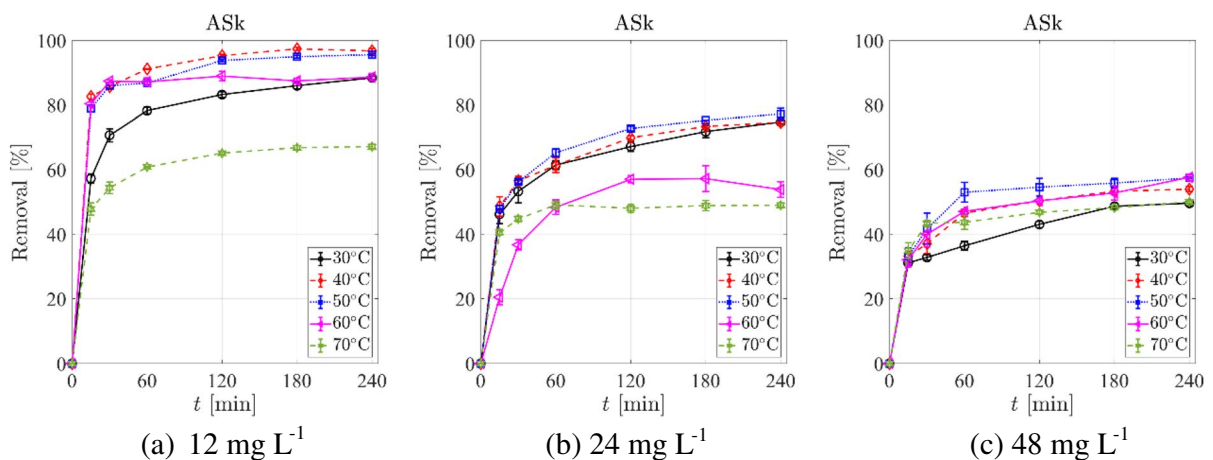

Fig. 12 Profiles removal dye RhB at pH 3: **a** 12, **b** 24, and **c** 48 mg L^{-1} of adsorbate and 2 g L^{-1} of adsorbent for different temperatures 30, 40, 50, 60, and 70 °C for ASk bioadsorbent
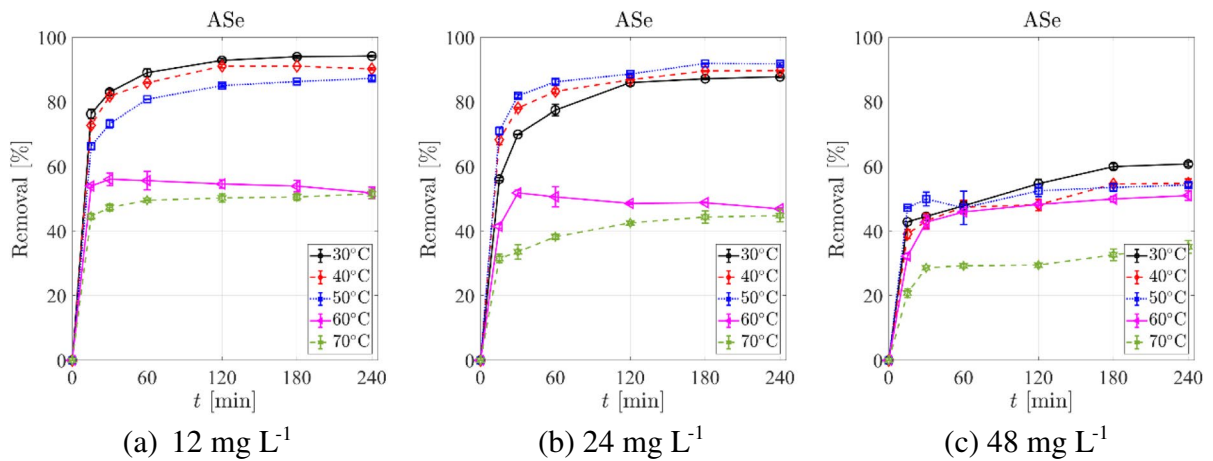
Fig. 13 Profiles removal dye RhB at pH 3: **a** 12, **b** 24 and **c** 48 mg L^{-1} of adsorbate and 2 g L^{-1} of adsorbent for different temperature 30, 40, 50, 60, and 70 °C for ASe bioadsorbent

and were evaluated using the following equations: (2) and (3)

$$\ln K_d = \frac{\Delta S^0}{R} - \frac{\Delta H^0}{RT} \qquad (2)$$

$$\Delta G^0 = -RT\ln K_d \qquad (3)$$

where R is the universal gas constant (8.314 J mol^{-1} K^{-1}), $K_d = \rho\, q_e / C_e$ represents the thermodynamic equilibrium constant, and T (in K) is the absolute temperature at which the experiment was performed (30, 40, 50, 60, and 70 °C). Given the low RhB concentration, we take the fluid density ρ as $\rho \approx \rho_{H_2O} = 1000$ g L^{-1}.

The change in enthalpy (ΔH^0) and entropy (ΔS^0) was obtained graphically from the ln K_d vs $1/T$ plot. The experimental data obtained for each RhB concentration (12, 24, and 48 mg L^{-1}) and temperature (30, 40, 50, 60, and 70 °C) were fitted to the model given by Eq. (2), to obtain the parameters ΔH^0, and ΔS^0. The values of the thermodynamic parameters

ΔH^0 and ΔS^0 are presented in Table 6, and the change in the Gibbs free energy in Table 7.

Table 6 shows that the adsorption process for ASe bioadsorbent is exothermic ($\Delta H^0 < 0$) and reversible ($\Delta S^0 < 0$) for the three adsorbate concentrations. Namely, as the adsorbate concentration increases, the amount of energy generated during the adsorption process decreases, and the process tends to become irreversible and stable. This behavior is more evident for the ASk bioadsorbent, where the nature of the process changes from exothermic to endothermic ($\Delta H^0 > 0$) and irreversible and stable ($\Delta S^0 > 0$) at a concentration of 48 mg L^{-1}. These findings are consistent with those observed in Sect. 3.2.4. In turn, the negative values in the Gibbs free energy change ($\Delta G^0 < 0$) presented in Table 7 indicate a feasible and spontaneous adsorption process in all cases for both bioadsorbents. Moreover, the decrease of the Gibbs free energy while temperature increases indicates that the adsorption process is more spontaneous and thus is more efficient at low temperatures.

Table 6 Enthalpy change and entropy change of ASk and ASe bioadsorbents

Adsorbate mg L^{-1}	ASk		ASe	
	ΔH^0, kJ mol^{-1}	ΔS^0, J/mol^{-1} K^{-1}	ΔH^0, kJ mol^{-1}	ΔS^0, J/mol^{-1} K^{-1}
12	-32.82 ± 7.29	-31.28 ± 0.07	-65.53 ± 0.50	-139.75 ± 1.68
24	-27.06 ± 0.15	-26.40 ± 0.57	-52.29 ± 0.30	-100.96 ± 0.99
48	1.86 ± 0.28	58.68 ± 0.76	-19.28 ± 0.71	-7.74 ± 1.39

Table 7 Gibbs free energy change in kJ mol^{-1} of ASk and ASe bioadsorbents

Adsorbate mg L^{-1}	T [K]				
	303	313	323	333	343
ASk					
12	-20.78 ± 0.01	-25.06 ± 0.02	-25.01 ± 0.03	-22.90 ± 0.01	-19.77 ± 0.01
24	-18.40 ± 0.02	-19.00 ± 0.01	-19.98 ± 0.05	-17.64 ± 0.07	-17.61 ± 0.01
48	-15.62 ± 0.04	-16.60 ± 0.05	-17.51 ± 0.08	-18.07 ± 0.01	-17.73 ± 0.01
ASe					
12	-22.68 ± 0.01	-21.97 ± 0.02	-21.88 ± 0.03	-17.42 ± 0.07	-17.90 ± 0.07
24	-20.63 ± 0.01	-20.49 ± 0.00	-23.18 ± 0.01	-16.87 ± 0.03	-17.13 ± 0.05
48	-16.77 ± 0.03	-16.69 ± 0.04	-17.15 ± 0.03	-17.33 ± 0.10	-15.98 ± 0.12

3.4 Kinetics Parameters

The study of adsorption kinetics is relevant as it provides information on the adsorption mechanism and extra- and intra-particle matter transfer phenomena that may control the adsorption rate, ultimately affecting the process efficiency. Pseudo-first- and pseudo-second-order kinetic models have been used to describe the adsorption process in an aqueous solution (Sahu & Singh, 2019). The study of adsorption kinetics is relevant as it provides information on the adsorption mechanism, which ultimately affects the process efficiency. Namely, extra- and intra-particle matter transfer phenomena may control the adsorption rate. Pseudo-first- and pseudo-second-order kinetic models have been used to describe the adsorption process in aqueous solution (Sahu & Singh, 2019).

The bioadsorption equilibrium time was analyzed using the methodology described in Sect. 2.5. Experimental data from the adsorption process, explained in Sect. 3.2, were fitted to both linearized kinetic models using the least squares method. The two kinetic models were pseudo-first-order (for physisorption process, Eq. (4)) and pseudo-second-order (for chemisorption, Eq. (5)) (Cheng et al., 2017; Pereira et al., 2021; Wang et al., 2020), given as

$$\ln\left(q_e - q_t\right) = \ln q_e - K_1 t \tag{4}$$

$$\frac{t}{q_t} = \frac{1}{K_2 q_e^2} + \frac{1}{q_e} t \tag{5}$$

where K_1 [min^{-1}] and K_2 [g mg^{-1} min^{-1}] are the pseudo-first- and pseudo-second-order adsorption equilibrium constants. In turn, q_e [mg g^{-1}] and q_t [mg g^{-1}] are the amount of RhB dye adsorbed at equilibrium and at a given time t, respectively, and can be obtained experimentally from the following expressions

$$q_e = \frac{\left(C_0 - C_e\right)V}{m} \tag{6}$$

$$q_t = \frac{\left(C_0 - C_t\right)V}{m} \tag{7}$$

with C_0 (mg L^{-1}) as the initial RhB dye concentration and C_t (mg L^{-1}) as the dye concentration at a time t (min). C_e (mg L^{-1}) is the RhB dye concentration at the adsorption equilibrium, m (g) is the bioadsorbent mass (for ASk or ASe), and V (L) is the total volume of the system.

The fitting of experimental results to the kinetic models, Eqs. (4) and (5) were performed for the results obtained for ASk and ASe adsorbents at the considered pH values (3, 5, 7, and 9), adsorbent concentrations (0.5 to 3 mg L^{-1}), adsorbate concentrations (6 to 72 mg L^{-1}), and temperatures (30, 40, 50, 60 and 70 °C). Tables 8 and 9 resume the kinetics parameters (K_1, K_2, and q_e), for ASk and ASe bioadsorbents using the pseudo-first-order and pseudo-second-order models. Fittings have coefficients of determination (R^2) higher than 0.9080 for the pseudo-first-order model and higher than 0.9504 for the pseudo-second-order model. The fittings to the pseudo-first- and second-order kinetic models for the different pH values, adsorbent and adsorbate concentrations, and temperatures are shown in Figs. S3-S8 in the SM.

Table 8 Kinetic parameters for the pseudo-first-order model for ASk and ASe bioadsorbents

	ASk			ASe		
Parameter	K_1, g mg^{-1} min^{-1}	q_e, mg g^{-1}	R^2	K_1, g mg^{-1} min^{-1}	q_e, mg g^{-1}	R^2
pH						
3	0.1161 ± 0.00005	5.1861 ± 0.0771	0.9895 ± 0.0027	0.1104 ± 0.0039	6.1916 ± 0.0189	0.9925 ± 0.0002
5	0.0694 ± 0.0046	3.8452 ± 0.0293	0.9922 ± 0.0034	0.0741 ± 0.0005	4.8028 ± 0.0342	0.9893 ± 0.0004
7	0.0650 ± 0.0048	4.0077 ± 0.1307	0.9738 ± 0.0050	0.0544 ± 0.0084	4.4141 ± 0.0085	0.9849 ± 0.0041
9	0.0687 ± 0.0032	3.6636 ± 0.3816	0.9513 ± 0.0057	0.0583 ± 0.0007	5.0896 ± 0.1386	0.9885 ± 0.0019
Bioadsorbent, g L^{-1}						
0.5	0.0543 ± 0.0041	8.3771 ± 0.7400	0.9531 ± 0.0086	0.0452 ± 0.0005	12.0396 ± 0.3874	0.9609 ± 0.0056
1.0	0.0419 ± 0.0031	6.7411 ± 0.4001	0.9596 ± 0.0254	0.0757 ± 0.0042	10.0852 ± 0.3887	0.9839 ± 0.0082
2.0	0.1161 ± 0.00005	5.1861 ± 0.0771	0.9895 ± 0.0027	0.1104 ± 0.0039	6.1916 ± 0.0189	0.9925 ± 0.0002
3.0	0.1025 ± 0.0027	3.1272 ± 0.3672	0.9932 ± 0.0001	0.1354 ± 0.0087	4.3571 ± 0.2618	0.9981 ± 0.0011
RhB, mg L^{-1}						
6	0.1182 ± 0.0125	2.7046 ± 0.0472	0.9936 ± 0.0018	0.1051 ± 0.0067	3.2423 ± 0.3276	0.9973 ± 0.0022
12	0.1161 ± 0.00005	5.1861 ± 0.0771	0.9895 ± 0.0027	0.1104 ± 0.0039	6.1916 ± 0.0189	0.9925 ± 0.0002
24	0.0602 ± 0.0108	7.1963 ± 0.1911	0.9695 ± 0.0042	0.0646 ± 0.0017	8.9900 ± 0.0717	0.9888 ± 0.0018
36	0.0586 ± 0.0003	9.4473 ± 0.1784	0.9142 ± 0.0018	0.1058 ± 0.0021	9.7273 ± 0.0762	0.9814 ± 0.0031
48	0.0563 ± 0.0022	8.9418 ± 0.3391	0.9220 ± 0.0150	0.0795 ± 0.0066	11.0929 ± 0.3634	0.9411 ± 0.0089
60	0.0280 ± 0.0009	12.2495 ± 0.1536	0.9904 ± 0.0004	0.0669 ± 0.0017	17.4377 ± 0.4233	0.9496 ± 0.0206
72	0.0241 ± 0.0013	11.4071 ± 0.0248	0.9932 ± 0.0020	0.0331 ± 0.0017	15.6982 ± 0.0150	0.9080 ± 0.0042
12 mg L^{-1}						
30	0.0694 ± 0.0027	5.1858 ± 0.0446	0.9895 ± 0.0016	0.1104 ± 0.0023	6.1917 ± 0.0109	0.9925 ± 0.0002
40	0.1308 ± 0.0014	6.3997 ± 0.0300	0.9900 ± 0.0009	0.1071 ± 0.0024	6.0378 ± 0.0650	0.9947 ± 0.00004
50	0.1231 ± 0.0041	5.7982 ± 0.0692	0.9904 ± 0.0004	0.0932 ± 0.0033	5.6042 ± 0.0611	0.9885 ± 0.00053
60	0.1636 ± 0.0118	5.8985 ± 0.0296	0.9996 ± 0.0001	0.8875 ± 0.8677	4.1304 ± 0.1190	0.9952 ± 0.00070
70	0.0793 ± 0.0069	3.8104 ± 0.0026	0.9861 ± 0.0006	0.1411 ± 0.0015	3.4048 ± 0.0716	0.9962 ± 0.00074
24 mg L^{-1}						
30	0.0601 ± 0.0063	7.1947 ± 0.1104	0.9695 ± 0.0024	0.0646 ± 0.0010	8.9900 ± 0.0414	0.9889 ± 0.00106
40	0.0670 ± 0.0074	7.2550 ± 0.0510	0.9698 ± 0.0046	0.0960 ± 0.0014	8.8015 ± 0.0308	0.9926 ± 0.00078
50	0.0584 ± 0.0006	7.0828 ± 0.0776	0.9776 ± 0.0006	0.1010 ± 0.0026	8.6901 ± 0.0137	0.9949 ± 0.00029
60	0.0332 ± 0.0012	6.8231 ± 0.2134	0.9936 ± 0.0023	0.1311 ± 0.0008	6.2318 ± 0.1775	0.9870 ± 0.00559
70	0.1159 ± 0.0000	6.3112 ± 0.0859	0.9966 ± 0.0012	0.0745 ± 0.0095	5.5812 ± 0.0812	0.9658 ± 0.00227
48 mg L^{-1}						
30	0.0563 ± 0.0013	8.9420 ± 0.1956	0.9223 ± 0.0092	0.0794 ± 0.0039	11.0930 ± 0.2100	0.9412 ± 0.00519
40	0.0539 ± 0.0034	13.7980 ± 0.3096	0.9718 ± 0.0070	0.0850 ± 0.0035	12.5295 ± 0.2422	0.9681 ± 0.00890
50	0.0533 ± 0.0066	14.2208 ± 0.7935	0.9918 ± 0.0060	0.1688 ± 0.0303	15.5727 ± 0.6041	0.9815 ± 0.01557
60	0.0541 ± 0.0071	13.4034 ± 0.1986	0.9741 ± 0.0027	0.0693 ± 0.0035	11.9466 ± 0.3375	0.9934 ± 0.00307
70	0.0869 ± 0.0053	10.8116 ± 0.2151	0.9878 ± 0.0074	0.0703 ± 0.0003	7.1907 ± 0.2109	0.9712 ± 0.0117

From Table 8 and 9, the fit has coefficients of determination (R^2) between 0.90 and 0.99. For the pseudo-second-order model (see Table 8 and 9), the lower coefficient of determination is 0.95.

From the data for pH, the highest pseudo-first- and pseudo-second-order kinetic constants, K_1 and K_2, are obtained at pH 3 for both bioadsorbents. The corresponding kinetic constants have comparable values for pH 5, 7, and 9. These results corroborate that the optimum pH value is 3, at which the highest adsorption rate is achieved.

Regarding the bioadsorbent concentration, a different behavior was observed for ASe and ASk. For seed, the higher the ASe concentration, the higher

Table 9 Kinetic parameters for the pseudo-second-order model for ASk and ASe bioadsorbents

Parameter	ASk			ASe		
	K_2, g mg^{-1} min^{-1}	q_e, mg g^{-1}	R^2	K_2, g mg^{-1} min^{-1}	q_e, mg g^{-1}	R^2
pH						
3	0.0470 ± 0.0035	5.6246 ± 0.0186	0.9996 ± 0.0001	0.0358 ± 0.0001	6.4823 ± 0.0174	0.9999 ± 0.00001
5	0.0185 ± 0.0018	4.0733 ± 0.0016	0.9995 ± 0.00005	0.0222 ± 0.0008	5.1803 ± 0.0415	0.9998 ± 0.0001
7	0.0196 ± 0.0029	4.4299 ± 0.0343	0.9989 ± 0.0006	0.0152 ± 0.0013	4.8792 ± 0.0035	0.9997 ± 0.0001
9	0.0154 ± 0.0004	4.2261 ± 0.2783	0.9958 ± 0.0015	0.0148 ± 0.0005	5.5826 ± 0.1121	0.9995 ± 0.0002
Bioadsorbent, g L^{-1}						
0.5	0.0068 ± 0.0002	9.4717 ± 0.5103	0.9959 ± 0.0018	0.0036 ± 0.0002	13.9098 ± 0.3963	0.9971 ± 0.0005
1.0	0.0062 ± 0.0009	7.7783 ± 0.1330	0.9966 ± 0.0030	0.0097 ± 0.0007	10.9865 ± 0.1990	0.9992 ± 0.0001
2.0	0.0470 ± 0.0035	5.6246 ± 0.0186	0.9996 ± 0.0001	0.0358 ± 0.0001	6.4823 ± 0.0174	0.9999 ± 0.00001
3.0	0.0602 ± 0.0003	3.2911 ± 0.2562	0.9999 ± 0.0001	0.0985 ± 0.0050	4.4618 ± 0.1699	1.0000 ± 0.0000
RhB, mg L^{-1}						
6	0.1034 ± 0.0021	2.8079 ± 0.0535	0.9995 ± 0.0002	0.0867 ± 0.0154	3.3476 ± 0.2074	0.9999 ± 0.00008
12	0.0470 ± 0.0035	5.6246 ± 0.0186	0.9996 ± 0.0001	0.0358 ± 0.0001	6.4823 ± 0.0174	0.9999 ± 0.00001
24	0.0086 ± 0.0012	8.1175 ± 0.0724	0.9983 ± 0.0006	0.0107 ± 0.0002	9.6805 ± 0.0187	0.9998 ± 0.00005
36	0.0082 ± 0.0002	10.3836 ± 0.1956	0.9601 ± 0.0007	0.0213 ± 0.0006	10.2136 ± 0.0656	0.9953 ± 0.00152
48	0.0048 ± 0.00007	10.5630 ± 0.1862	0.9940 ± 0.0016	0.0056 ± 0.00009	12.7659 ± 0.1873	0.9966 ± 0.00125
60	0.0023 ± 0.0001	14.3419 ± 0.1223	0.9958 ± 0.0004	0.0057 ± 0.00002	18.8424 ± 0.3435	0.9788 ± 0.01211
72	0.0020 ± 0.0002	13.5981 ± 0.1223	0.9978 ± 0.0007	0.0025 ± 0.00017	17.7313 ± 0.0871	0.9504 ± 0.00149
12 mg L^{-1}						
30	0.0209 ± 0.00114	5.5639 ± 0.0312	0.9993 ± 0.00013	0.0387 ± 0.00132	6.4547 ± 0.0055	0.9995 ± 0.00009
40	0.0487 ± 0.00006	6.6369 ± 0.0329	0.9979 ± 0.00044	0.0385 ± 0.00118	6.2925 ± 0.0599	0.9994 ± 0.00035
50	0.0486 ± 0.00239	6.0261 ± 0.0626	0.9974 ± 0.00029	0.0314 ± 0.00140	5.9016 ± 0.0547	0.9989 ± 0.00014
60	0.1177 ± 0.02357	5.9910 ± 0.0125	0.9988 ± 0.00020	$- - - - - - - -$	4.1235 ± 0.1128	0.9948 ± 0.00122
70	0.0353 ± 0.00445	4.0540 ± 0.0141	0.9988 ± 0.00028	0.1185 ± 0.00379	3.5004 ± 0.0772	0.9993 ± 0.00034
24 mg L^{-1}						
30	0.0118 ± 0.00153	7.8292 ± 0.0695	0.9930 ± 0.00107	0.0108 ± 0.00025	9.6859 ± 0.0293	0.9992 ± 0.00033
40	0.0136 ± 0.00224	7.8480 ± 0.0111	0.9930 ± 0.00198	0.0212 ± 0.00034	9.2440 ± 0.0297	0.9996 ± 0.00010
50	0.0117 ± 0.00037	7.6966 ± 0.0940	0.9969 ± 0.00028	0.0239 ± 0.00116	9.0882 ± 0.0009	0.9995 ± 0.00007
60	0.0053 ± 0.00013	7.7960 ± 0.2081	0.9780 ± 0.00509	0.0850 ± 0.00800	6.3108 ± 0.1538	0.9759 ± 0.00726
70	0.0457 ± 0.00009	6.5245 ± 0.0825	0.9979 ± 0.00016	0.0209 ± 0.00303	5.9890 ± 0.0600	0.9897 ± 0.00130
48 mg L^{-1}						
30	0.0083 ± 0.00032	9.8373 ± 0.2099	0.9660 ± 0.00637	0.0105 ± 0.00067	11.9728 ± 0.2289	0.9750 ± 0.00444
40	0.0055 ± 0.00031	15.0435 ± 0.2908	0.9921 ± 0.00471	0.0112 ± 0.00076	13.3563 ± 0.1957	0.9872 ± 0.00470
50	0.0053 ± 0.00076	15.4833 ± 0.6817	0.9946 ± 0.00112	0.0306 ± 0.00606	16.0156 ± 0.6128	0.9855 ± 0.01389
60	0.0054 ± 0.00087	14.7083 ± 0.0966	0.9912 ± 0.00367	0.0091 ± 0.00030	12.8024 ± 0.3420	0.9959 ± 0.00286
70	0.0143 ± 0.00177	11.4467 ± 0.1417	0.9942 ± 0.00313	0.0145 ± 0.00099	7.7526 ± 0.2610	0.9784 ± 0.00348

the pseudo-first- and second-order kinetic constants, with maximums of 0.1354 ± 0.0087 min^{-1} and 0.0985 ± 0.0050 g mg^{-1} min^{-1}, respectively, for a concentration of 3 mg L^{-1}. For the ASk bioadsorbent, a minimum is observed in both models for a concentration of 1 g L^{-1}. In the first-order model, the maximum of K_1 occurs at 2 g L^{-1} (0.1161 ± 0.00005 min^{-1}), while K_2 is maximum at 3 g L^{-1} (0.0602 ± 0.0003 g mg^{-1} min^{-1}) in the second-order-model. In addition, the bioadsorbent's equilibrium bioadsorption capacity reduces with increasing the bioadsorbent concentration. In Enahoro Agarry ([2016](#)), the authors reported a similar behavior. This is due the larger amount of

adsorbent, which provides a larger surface area for the same amount of adsorbate, resulting in less adsorbate per gram of adsorbent.

In turn, from the results for RhB concentration, we observe for both bioadsorbents that the equilibrium bioadsorption capacity increased monotonically with the initial RhB dye concentration from 6 to 60 mg L^{-1} (see Table 8 and 9). Nevertheless, q_e decreases for 72 mg L^{-1}, which can be attributed to increased competition of RhB molecules for the available active sites. To say, lower competition for the surface active sites at low adsorbate concentrations leads to a higher adsorption rate and vice versa. Note that for both bioadsorbents, the pseudo-first kinetic model led to similar values for K_1 at RhB concentrations of 6 and 12 mg L^{-1} (considering the corresponding standard deviation). On the other hand, for the ASk bioadsorbent, the values of the pseudo-first- and second-order adsorption constants decrease with increasing RhB adsorbate concentration (see Table 8 and 9). From these results, the pseudo-second-order model better describes the behavior of the process for both bioadsorbents (see Fig. S5 in SM) (Enahoro Agarry, 2016). The inverse relation between most of the adsorbate concentrations and their corresponding kinetic values is similar to that obtained by Inyinbor et al. (2015). In their work, (Inyinbor et al., 2015) studied the RhB removal with activated *Irvingia gabonensis* bioadsorbents at pH 3, 50 mg L^{-1} of RhB, and with an adsorbent concentration of 1 g L^{-1}. The reported values of the pseudo-first- and second-order kinetic constants were 0.019 min^{-1} and 0.006 mg g^{-1} min^{-1}, respectively. In this work, under similar conditions (a concentration of RhB and ASk of 48 mg L^{-1} and 2 g L^{-1} at pH 3), K_1 and K_2 were 0.0563 min^{-1} and 0.048 mg g^{-1} min^{-1}, respectively. For the pseudo-first-order kinetic model, the kinetic constants are in the same order of magnitude, with a faster adsorption rate for ASk than with *Irvingia gabonensis*. Moreover, the constant values have a different order of magnitude for the pseudo-second-order model. This may be due to the mass transfer limitations of the activated bioadsorbent since it is a porous material.

Exploring five different temperatures for three RhB concentrations showed that skin-derived bioadsorbent was more affected than seed bioadsorbent during adsorption. For ASk, the equilibrium adsorption capacity, q_e, has no significant change in the temperature range from 30 to 60 °C for 12 and 24 mg

L^{-1} adsorbate concentrations, after which a decrease is observed. For 48 mg L^{-1}, a higher variation is observed for temperatures below 50 °C and after this value, which is also observed for Ase. For ASe, higher equilibrium adsorption capacities are obtained for 12 and 24 mg L^{-1} adsorbate concentrations. On the other hand, for the ASk and ASe bioadsorbent, the adsorption rate is not influenced significantly. Although the kinetic constants present variations, they are within the average deviation (see Table 8 and 9). Nevertheless, all adsorbent concentration cases exhibited similar behavior in which the adsorption capacity (better shown in Figs. S6-S8 in the SM) presents a maximum at a given temperature at 40 or 50 °C, depending on the experimental conditions.

Finally, exploring five different temperatures allowed us to identify that the adsorption process is more affected for the skin-derived bioadsorbent than for seed bioadsorbent. For the ASk bioadsorbent, the equilibrium adsorption capacity, q_e, for 12 and 24 mg L^{-1} adsorbate concentrations has no significant change in the temperature range from 30 to 60 °C. For a temperature of 70 °C, in Table 8 and 9, a decrease in the value of q_e were observed. While for 48 mg L^{-1}, it observes that an increase in temperature from 30 to 40 °C increases the amount of adsorbed dye. However, for higher temperatures, there are no changes in the values that are not observable; even at 70 °C, the value of q_e also decreases, as occurred with 12 and 24 mg L^{-1}.

For ASk and ASe bioadsorbents, both kinetic models exhibit a maximum absorption rate at 60–70 °C. On the other hand, for the ASk and ASe bioadsorbent, the adsorption rate is not influenced significantly. Although the kinetic constants present variations, they are within the average deviation (see Table 8 and 9). Figures S6-S8 compare the experimental (marker) and theoretical (dashed and solid lines) bioadsorption capacity of skin (left column) and seed (right column).

Avocado waste has also been used to remove other dyes. Bazzo et al. (2015) studied the removal of crystal violet dye with a natural bioadsorbent from waste avocado seed at pH 7 and 25 °C. For this experiment, the authors considered a dye concentration of 50 mg L^{-1} and an adsorbent concentration of 4 g L^{-1}. They report the kinetic constants for a pseudo-first- and pseudo-second-order models as 0.2154 min^{-1} and 0.03080 g mg^{-1} min^{-1} with determination coefficients

close to unity. In turn, Asiagwu et al. (2017) investigated the amaranth dye removal in the presence of 40 mg L^{-1} of the waste avocado seed, for which they determined the corresponding kinetic constants as 0.057 min^{-1} (R^2=0.336) for pseudo-first-order and 30.94 g mg^{-1} min^{-1} (R^2=0.999) for the pseudo-second-order model. In our work for ASe with a concentration of RhB of 48 mg L^{-1}, K_1=0.0795±0.0066 min^{-1} and K_2=0.0056±0.00009 g mg^{-1} min^{-1}. As observed, the values of K_1 are consistent with those reported in the literature, but K_2 obtained in Asiagwu et al. (2017) and Bazzo et al. (2015) are higher than in our case. This can be explained by the higher bioadsorbent concentration used by the authors, in contrast to the concentration used in this work, which implies more sites available on the adsorbent surface. In Mallampati et al. (2015), the authors studied the bioadsorption of the dyes alcian blue, methylene blue, neutral red, and brilliant blue using activated avocado skin. Their experimental conditions were pH 7, 30 °C, 100 mg L^{-1} of adsorbate, and 10 g L^{-1} of adsorbent. The values they obtained for K_2 ranged from 0.0033 to 0.0432 g mg^{-1} min^{-1}. In turn, Netto et al. (2019) studied methylene blue (100 mg L^{-1}) adsorption by avocado seeds (1 g L^{-1}). They reported pseudo-first- and pseudo-second-order adsorption kinetics of 0.095 min^{-1} (R^2=0.995) and 0.0016 g mg^{-1} min^{-1} (R^2=0.994), respectively. The values reported by Mallampati et al. (2015) and Netto et al. (2019) agree with those reported in our work (see Table 8 and 9).

Finally, from the adsorption capacity plot as a function of time, shown in Figs. S3-S8 in SM, it is observed that during the first minutes of contact (within the first 15–30 min), the adsorption capacity increases rapidly due to a large number of available binding sites. This process is followed by a slowdown in the absorption capacity, leading to a plateau caused by the saturation of adsorption sites. It is noteworthy to highlight three facts: (i) for the majority of the experimental conditions of both bioadsorbents, around 70–90% removal (of the adsorption/desorption equilibrium) is reached within the first hour of contact; (ii) under similar conditions, seed-derived material owns a higher adsorption capacity than ASk due to its higher surface area; and (iii) the pseudo-second-order kinetic model represents more precisely the experimental behavior of the ASk and ASe bioadsorbents. Similar results have been reported by Mallampati (2015) for activated avocado skin and other adsorbents (Aichour et al., 2018; Bello et al., 2015; Berrazoum et al., 2015). From the above results, it is possible to elucidate that the adsorption mechanism is dominated by chemisorption.

3.5 Adsorption Isotherm Model

Adsorption isotherm models are valuable in designing absorption processes and optimizing adsorbent usage. These models rely on the adsorption properties and equilibrium data that have been determined experimentally and depend on the physicochemical conditions of the interactions (Naderir, 2015). In this work, the Freundlich and Langmuir models, given by Eqs. (8) and (9), were used to evaluate the maximum adsorption capacity of the bioadsorbents. The experimental data were obtained from the results of the bioadsorption process at equilibrium, considering pH 3, 2 g L^{-1} of ASk or ASe adsorbents, and different RhB concentrations (6 to 72 mg L^{-1}).

$$\ln q_e = \ln K_F + \frac{1}{n}\ln C_e \tag{8}$$

$$\frac{1}{q_e} = \frac{1}{q_{max}} + \frac{1}{q_{max}K_L} \tag{9}$$

The fitting parameters for the Langmuir and Freundlich models are given in Table 10 and 11, respectively, for both biomaterials. The results show a better fitting of the Langmuir model for both bioadsorbents. This indicates that the adsorption process of the RhB dye molecules on the bioadsorbent is a monolayer. Namely, the interaction between the groups on ASe and ASk bioadsorbents (see Figs. 3, 4, and

Table 10 Langmuir adsorption parameters of ASk and ASe bioadsorbents

Bioadsorbent	q_{max} [mg g^{-1}]	K_L [L mg^{-1}]	R^2
ASk	13.1240±0.0806	0.3548±0.0021	0.8907±0.0027
ASe	17.9998±0.6233	0.7443±0.0316	0.9606±0.0009

Table 11 Freundlich adsorption parameters of ASk and ASe bioadsorbents

Bioadsorbent	n	K_F	R^2
ASk	0.6966 ± 0.0042	1.3559 ± 0.0003	0.8118 ± 0.0038
ASe	0.5614 ± 0.0041	1.3451 ± 0.0048	0.9382 ± 0.0033

5) and RhB molecules play a key role in the effective adsorption.

From the Langmuir model (see Table 10), the monolayer adsorption capacity (q_{max}) for ASk and ASe are 13.1240 ± 0.0806 and 17.9998 ± 0.6233 mg g^{-1}, respectively. A higher adsorption capacity is obtained for the ASe bioadsorbent, which can be attributed to its higher number of functional groups, such as carbonyl, carboxyl, esters, ether, methoxy, and hydroxyl (see Table 3 and 4), since it contains lignin, cellulose, and hemicellulose. As for the ASk bioadsorbent, the functional groups are mainly C–O and C–OH (see Table 3 and 4) for its lower lignin content. This decrease in the functional groups of ASk leads to lower adsorption capacity. For comparison, Table 12 presents the maximum adsorption capacity for different absorbates and natural or activated bioadsorbents. The corresponding concentrations are provided for each case. Note that the high maximum adsorption capacities reported for several materials correspond to activated and structured bioadsorbents that inherently own larger surface areas than natural bioadsorbents (as in this work). Nevertheless, the maximum adsorption capacity for ASk and ASe agrees with reported results under similar conditions.

In addition to previous parameters, it is important to determine whether the adsorption process is favorable. This can be accomplished by the separation factor R_L (also referred to as the equilibrium parameter), given by Eq. (10)

$$R_L = \frac{1}{1 + K_L C_0} \tag{10}$$

Table 12 Maximum adsorption capacity

Adsorbate	[mg L^{-1}]	Bioadsorbent	[g L^{-1}]	q_{max} [mg g^{-1}]	Author
RhB	6–72	ASk	2	13.2040	This work
RhB	6–72	ASe	2	17.9998	This work
RhB	10	Activated carbon	0.1–0.5	253.81–294.98	Liu et al. (2022)
RhB	10–40	Activated *Irvingia gabonensis*	1–5	212.77–232	Inyinbor et al. (2015)
RhB	200–1000	Activated *Gmelina aborea* leaves	1	142.86	Bello et al. (2015)
Reactive orange	50–150	Municipal solid waste	2.5	45.84	Berrazoum et al. (2015)
Methylene blue	10–50	Seed husk of Timbaúva	20	3.62	Lima et al. (2020)
Crystal violet	25	Avocado seed	4	75.19–80.15	Bazzo et al. (2015)
Amaranth red	10–50	Avocado seed	40	0.57	Asiagwu et al. (2017)
Methylene blue	100	Avocado seed	0.295–1.705	77.34	Netto et al. (2019)
Methyl orange	10–70	Activated avocado seed	5	0.1	Asiagwu et al. (2013)
Dyes (AB, MB, NR, BB)	5–200	Activated avocado skin	10	6.88–62.11	Mallampati et al. (2015)
Dyes (AB, MB, NR, BB)	5–200	Activated hamimelon skin	10	6.311–66.55	Mallampati et al. (2015)
Dyes (AB, MB, NR, BB)	5–200	Activated dragon fruit skin	10	13.68–71.85	Mallampati et al. (2015)
Methylene blue	25–300	Activated lemon peels	0.025–2.2	208.64	Aichour et al. (2018)
Methylene blue	100	Activated lemon peels/alginate beads	0.025–2.2	841.37	Aichour et al. (2018)
Anionic dye	10–100	3D porous bioadsorbents	0.1	2015–2297	Mokhtari et al. (2021)
Anthracene	50–250	Unripe plantain peels	0.2–2.0	27.70	Enahoro Agarry (2016)
Phenolic compounds	–	Activated avocado seed	–	406.9–454.5	Leite et al. (2017)
Acetaminophen	20	Grape stalk	3–30	2.18 ± 0.05	Villaescusa et al. (2011)

with C_0 as the initial adsorbate concentration and K_L as the Langmuir constant, related to the adsorption energy. If $0 < R_L < 1$, the process is favorable. The process is irreversible if $K_L \gg 1$ ($R_L \sim 0$) and linear if $K_L = 0$ ($R_L = 1$).

We consider that the adsorbate concentrations used in this investigation, from 6 to 72 mg L^{-1}, leads to a separation factor of $0.0376 \leq R_L \leq 0.3196$ for ASk and $0.0183 \leq R_L \leq 0.183$ for ASe, respectively. Since R_L is in the range 0–1, it confirms the favorable removal of the RhB process under the explored conditions. In addition, lower R_L values at higher RhB dye concentrations suggest that the absorption was more favorable for these conditions as it approaches the irreversible condition ($R_L \rightarrow 0$). This is consistent with the results obtained from the thermodynamic analysis, Sect. 3.3: the process tends to be irreversible for higher adsorbate concentrations (see Table 6). In Asiagwu et al. (2013) and Mallampati et al. (2015), the authors reported a favorable adsorption process using avocado seed and skin, with values of $0.008 \leq R_L \lesssim 1$, consistent with our results.

3.6 Adsorption Mechanisms

As described in Sect. 3.1.8, the pH values at the IEP are 5.09 and 4.50 for ASk and ASe, respectively. Below these pH values (pH 3 in our case), the surface of the bioadsorbent is positively charged, and zwitterions of RhB ($pK_a = 3.7$) coexist. Therefore, the adsorption mechanism of RhB onto the bioadsorbent is likely due to electrostatic interaction between the positively charged surface of the bioadsorbent and the negatively charged carboxyl groups of RhB. After the adsorption process, FT-IR analysis of the bioadsorbent samples confirmed the findings. Figure 14 compares the FT-IR spectra before and after the adsorption process. A band of higher intensity assigned to the carboxyl group (at 1650 cm^{-1}) was identified in FT-IR spectra of both bioadsorbents after the adsorption process. At 1590 cm^{-1}, a group can be associated with the NH amino group of RhB adsorbed on the bioadsorbents. The presence of C–O (923 cm^{-1}) and –C–O–C (1180 cm^{-1}) groups can be attributed to π-π interactions with functional groups.

3.7 Reusability

Applying the adsorption process in pollutant removal requires materials to be stable under operation conditions and reuse (cycling). Figure 15 compares the RhB dye removal by ASk and ASe bioadsorbents. The stability study was performed for five cycles with a contact time of 240 min each. The experiments were carried out at pH 3, a concentration of 2 g L^{-1} of bioadsorbent and 12 mg L^{-1} of RhB, as detailed in Sect. 2.5. At the end of the adsorption process, the bioadsorbent (ASk and ASe) was recovered, dried at room temperature, and used in the next experiment. This procedure was repeated for each cycle. As observed, the removal rate of ASk bioadsorbent decreases from 88.41 in the first cycle to 75.50% in the fifth cycle, with a similar percentage (~80%) in the second, third, and fourth cycles. As for the ASe bioadsorbent, the removal dropped from 91.19% in the first cycle to 78.10% in the last one, which in most cases outperformed the removal of ASk biomaterial.

Figure 16 shows the micrograph of the materials after the adsorption process at pH 3. As can be seen, the morphology of both bioadsorbents changes

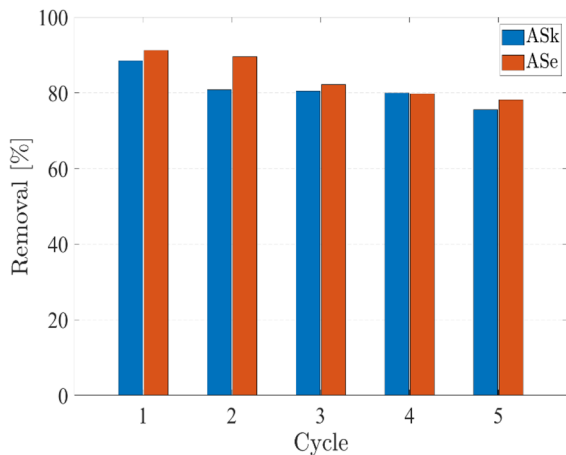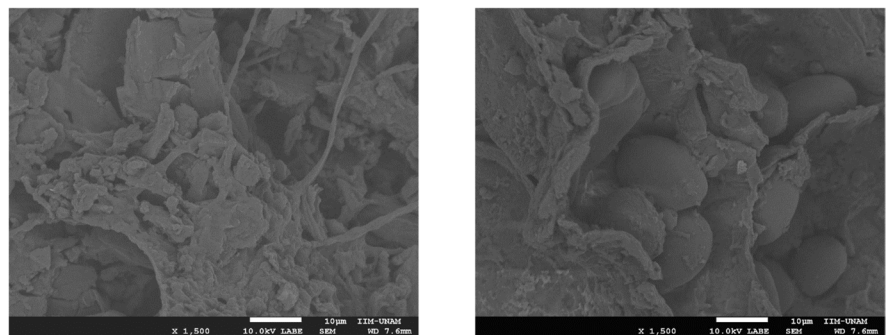**Fig. 14** Comparison of FT-IR spectra before and after the adsorption process for **a** ASk and **b** ASe bioadsorbent

(a) ASk

(b) ASe
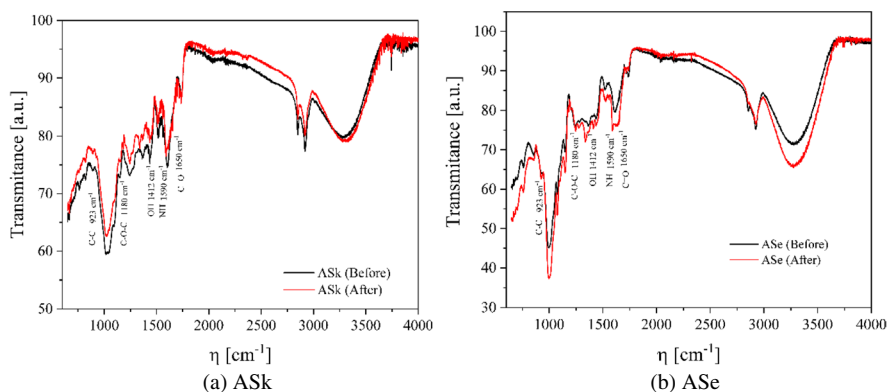
Fig. 15 Removal dye RhB at pH 3, 12 mg L^{-1} of adsorbate, and 2 g L^{-1} at 30 °C for five cycles of reusability for skin and seed bioadsorbents

from smooth spheres (see Fig. 7) to fibrous structures. This can be attributed to the decomposition of the cellulose polymers and leaching processes during the adsorption process at the experimental conditions (temperature and pH) (Costa et al., 2021).

After several adsorption cycles, the bioadsorbent will exhaust until it reaches the desired performance, and in this case, the spent bioadsorbent must be regenerated for further reuse. The regeneration processes involve solvent (Inyinbor et al., 2015; Mokhtari et al., 2021; Yadav et al., 2022), wash (Yadav et al., 2022), acid (Bello et al., 2015; Gupta & Jain, 2021) or caustic wash (Mallampati et al., 2015; Mokhtari et al., 2021), stream activation, and thermal regeneration (Sahu & Singh, 2019). It is worth mentioning that the regeneration process can be a source of contamination if suitable treatment is not implemented

(Zhang et al., 2023). It is important to emphasize that the selection of the regeneration process for a natural bioadsorbent must be carried out under chemical and thermal conditions that guarantee the permanence of the properties of the bioadsorbent and its effectiveness in the removal process.

To establish a suitable methodology for the final disposal of the bioadsorbent, we must consider the adsorbate it contains. The methods that have been proposed include disposal in a landfill, incineration, and discharging into the ocean. However, the most used is landfill, since for incineration and discharge in the ocean, one must consider the cost of energy required to burn adsorbent and the regulatory restrictions on ocean disposal (Sahu & Singh, 2019).

4 Conclusions

The recovery and valorization of avocado processing by-products through novel sustainable approaches allow for converting these residues into high-value products, reducing their accumulation, disposal, and adverse environmental problems. This work evaluated the removal of RhB dye by the bioadsorption process. For this purpose, bioadsorbents derived from avocado skin (ASk) and seed (ASe) were synthesized by simple processes which can incorporate green energy technologies, such as solar drying for dehydration processes. ASk and ASe bioadsorbents were applied to remove rhodamine B under different experimental conditions for pH, dye concentration, bioadsorbent concentration, and temperature. The results of bioadsorption showed efficacy in the removal of the dye RhB. The highest percentages of dye removal were at pH 3 and 2 g L^{-1} of bioadsorbent.

Fig. 16 Microscopy of **a** ASk and **b** ASe spent bioadsorbents

(a) ASk

(b) ASe

The pseudo-second-order kinetic model can be successfully adopted to describe the bioadsorption process. The adsorption isotherm was fitted by the Langmuir and Freundlich models, with a better fitting by the Langmuir isotherm. The adsorption capacity of the RhB on ASk and ASe are 13.1240 and 17.9998 mg g^{-1} obtained at 30 °C and pH 3. The adsorption of RhB on ASk and Ase bioadsorbents is spontaneous, exothermic, and reversible. The results show that adsorption is more efficient at lower temperatures (30 °C).

Recycling the seed and skin of avocado peels is efficient and can be used in consecutive pollutant adsorption studies without considerable losses in their adsorption capacities at pH 3 and a temperature of 30 °C. ASk and ASe bioadsorbents are economically and environmentally viable alternatives for wastewater treatment in several production sectors or as a process to remove trace contaminants in water treatment plants.

Author Contribution Conceptualization: Sayra Orozco, Michel Rivero, and Jaime Espino. Sayra Orozco and Michel Rivero wrote the first draft of the manuscript. Methodology: Sayra Orozco, Michel Rivero, Esteban Montiel, Jaime Espino, and Roberto Guerra. Sayra Orozco and Michel Rivero performed the investigation, validation, software, and visualization. All authors contributed to writing, reviewing, and editing, and thus, all authors agreed to the published version of the manuscript.

Data availability All data generated or analyzed during this study are included in this published article.

Declarations

Conflict of interest The authors declare no competing interests.

Ethical approval and consent to participate Not applicable.

Consent for publication Not applicable.

References

Adegoke, K. A., & Bello, O. S. (2015). Dye sequestration using agricultural wastes as adsorbents. *Water Resources and Industry, 12*, 8–24. https://doi.org/10.1016/j.wri.2015.09.002

Ahmad, T., & Danish, M. (2022). A review of avocado waste-derived adsorbents: Characterizations, adsorption characteristics, and surface mechanism. *Chemosphere, 296*, 134036. https://doi.org/10.1016/j.chemosphere.2022.134036

Aichour, A., Zaghouane-Boudiaf, H., Viseras Iborra, H., & Sanchez Polo, M. (2018). Bioadsorbent beads prepared from activated biomass/alginate for enhanced removal of cationic dye from water medium: Kinetics, equilibrium and thermodynamic studies. *Journal of Molecular Liquids, 256*, 533–540. https://doi.org/10.1016/j.molliq.2018.02.073

Aksu, Z., & Tezer, S. (2000). Equilibrium and kinetic modelling of biosorption of Remazol Black B by Rhizopus arrhizus in a batch system: Effect of temperature. *Proc. Biochem., 36*, 431–439. https://doi.org/10.1016/S0032-9592(00)00233-8

Albanio, I. I., Muraro, P. C. L., & da Silva, W. L. (2021). Rhodamine B dye adsorption onto biochar from olive biomass waste. *Water, Air, and Soil Pollution, 232*(5). https://doi.org/10.1007/s11270-021-05110-6

Al-Gheethi, A. A., Azhar, Q. M., Kumar, P. S., Yusuf, A. A., Al-Buriahi, A. K., Mohamed, R. M. S. R., & Al-shaibani, M. M. (2022). Sustainable approaches for removing Rhodamine B dye using agricultural waste adsorbents: A review. *Chemosphere, 287*, 132080. https://doi.org/10.1016/j.chemosphere.2021.132080

Araújo, T., Parnell, A.-J., Bernardo, G., & Mendes, A. (2023). Cellulose-based carbon membranes for gas separations - Unraveling structural parameters and surface chemistry for superior separation performance. *Carbon, 204*, 398–410. https://doi.org/10.1016/j.carbon.2022.12.062

Arivoli, S., Thenkuzhali, M., & Prasath, M. D. (2009). Adsorption of rhodamine B by acid activated carbon-Kinetic, thermodynamic and equilibrium studies. *Orbital: The Electronic Journal of Chemistry, 1*. https://doi.org/10.17807/orbital.v1i2.24

Asiagwu, A. K., Omuku, P. E., & Alisa, C. O. (2013). Kinetic model for the removal of methyl orange (dye) from aqueous solution using avocado pear (Persea Americana) seed. *Journal of Chemical, Biological and Physical Sciences, 3*, 48–57.

Asiagwu, A. K., Okposo, M. A., Peretomo-Clarke, M. A., & Ojebah, C. K. (2017). Kinetic model for the removal of amaranth dye from aqueous solution using avocado pear seed as biomass. *International Journal of Innovation in Science and Mathematics, 5*, 119–123.

Bahsaine, K., Chakhtouna, H., Mekhzoum, M. E. M., Zari, N., Benzeid, H., Qaiss, A. el kacem, & Bouhfid, R. (2023). Efficient cadmium removal from industrial phosphoric acid using banana pseudostem-derived biochar. *Biomass Conversion and Biorefinery*, 1–15. https://doi.org/10.1007/s13399-023-04130-y

Balbay, S., & Acıkgoz, C. (2022). New method for producing carbon sphere from waste tyre (NEWCSWT). *Waste and Biomass Valorization, 13*, 4951–4962. https://doi.org/10.1007/s12649-022-01765-2

Bangar, S. P., Dunno, K., Dhull, S. B., Siroha, A. C., Changan, S., Maqsood, S., & Rusu, A. V. (2022). Avocado seed discoveries: Chemical composition, biological properties, and industrial food applications. *Food Chemistry, 16*, 100507. https://doi.org/10.1016/j.fochx.2022.100507

Bazzo, A., Adebayo, M. A., Dias, S. L. P., Lima, E. C., Vaghetti, J. C. P., de Oliveira, E. R., Leite, A. J. B., & Pavan, F. A. (2015). Avocado seed powder: Characterization and its application for crystal violet dye removal from aqueous solutions. *Desalination and Water Treatment, 57*, 1–16. https://doi.org/10.1080/19443994.2015.1074621

Bello, O. S., Alabi, E. O., Adegoke, K. A., Adegboyega, S. A., Inyinbor, A. A., & Dada, A. O. (2015). Rhodamine B dye sequestration using Gmelina aborea leaf powder. *Heliyon, 6*, e02872. https://doi.org/10.1016/j.heliyon.2019.e02872

Berrazoum, A., Marouf, R., Ouadjenia, F., & Schott, J. (2015). Bioadsorption of a reactive dye from aqueous solution by municipal solid waste. *Biotechnology Reports, 7*, 44–50. https://doi.org/10.1016/j.btre.2015.04.005

Besegatto, S. V., Martins, M. L., Lopes, T. J., & da Silva, A. (2021). Multivariated calibration as a tool for resolution of color from mandarin peel and dyes in aqueous solution for bioadsorption studies. *Journal of Environmental Chemical Engineering, 9*, 104605. https://doi.org/10.1016/j.jece.2020.104605

Boeykens, S. P., Redondo, N., Alvarado, O. R., Caracciolo, N., & Vázquez, C. (2019). Chromium and lead adsorption by avocado seed biomass study through the use of total reflection X-ray fluorescence analysis. *Applied Radiation and Isotopes, 153*, 108809. https://doi.org/10.1016/j.apradiso.2019.108809

Boeykens, S. P., Saralegui, A., Caracciolo, N., & Piol, M. N. (2018). Agroindustrial waste for lead and chromium biosorption. *Journal of Sustainable Development of Energy, Water and Environment Systems, 6*, 341–350. https://doi.org/10.13044/j.sdewes.d5.0184

Cheng, S., Zhang, L., Xia, H., Peng, J., Shu, J., Li, C., Jiang, X., & Zhang, Q. (2017). Adsorption behavior of methylene blue onto waste derived adsorbent and exhaust gases recycling. *RSC Advances, 7*, 27331. https://doi.org/10.1039/C7RA01482A

Costa, M. E. G., da Costa-Assunao, F. P., Teribele, T., Pereira, L. M., de Castro, D. A. R., Santo, M. C., da Costa, C. E. F., Shultze, M., Hofmann, T., & Machado, N. T. (2021). Characterization of bio-adsorbents produced by hydrothermal carbonization of corn stover: Application on the adsorption of acetic acid from aqueous solutions. *Energies, 14*, 8154. https://doi.org/10.3390/en14238154

de Difusión y Publicaciones, D. G. (2021). *Ley General de Economía Circular*

Denvir, A. (2023). Avocado expansion and the threat of forest loss in Michoacan, Mexico under climate change scenarios. *Applied Geography, 151*, 102856. https://doi.org/10.1016/j.apgeog.2022.102856

di Bitonto, L., Reynel-Ávila, H. E., Mendoza-Castillo, D. I., Bonilla-Petriciolet, A., & Pastore, C. (2021). Residual Mexican biomasses for bioenergy and fine chemical production: Correlation between composition and specific applications. *Biomass Conversion and Biorefinery, 11*, 619–631. https://doi.org/10.1007/s13399-020-00616-1

Duque-Acevedo, M., Belmonte-Urena, L. J., Cortés-García, J., & Camacho-Ferre, F. (2020). Agricultural waste: Review of the evolution, approaches and perspectives on alternative uses. *Global Ecology and Conservation, 22*, e00902. https://doi.org/10.1016/j.gecco.2020.e00902

Elizalde González, M. P., Mattusch, J., Pelaéz Cid, A. A., & Wennrich, R. (2007). Characterization of adsorbent materials prepared from avocado kernel seeds: Natural, activated and carbonized forms. *Journal of Analytical and Applied Pyrolysis, 78*, 185–193. https://doi.org/10.1016/j.jaap.2006.06.008

Enahoro Agarry, S. (2016). Anthracene bioadsorption from simulated wastewater by chemically-treated unripe plantain peel bioadsorbent: Batch kinetics and isothermal modeling studies. *Polycyclic Aromatic Compounds, 39*. https://doi.org/10.1080/10406638.2016.1255650

Fan, H., Ma, Y., Wan, J., & Wang, Y. (2020). Removal of gentian violet and rhodamine B using banyan aerial roots after modification and mechanism studies of differential adsorption behaviors. *Environmental Science and Pollution Research, 27*, 9152–9166. https://doi.org/10.1007/s11356-019-07024-7

Foroutan, R., Reza, Mohammadi, Farjadfard, Z., Esmaeili, H., Saberi, M., Sahebi, S., Dobaradaran, S., & Ramavan, B. (2019). Characteristics and performance of Cd Ni, and Pb bio-adsorption using Callinectes sapidus biomass: Real wastewater treatment. *Environmental Science and Pollution Research, 26*, 6336–6347. https://doi.org/10.1007/s11356-018-04108-8

Gómez-Tagle, A. F., Gómez-Tagle, A., Fuerte-Velázquez, D. J., Barajas-Alcalá, A. G., Quiroz-Rivera, F., Alarcón-Chaires, P. E., & Guerrero-García-Rojas, H. (2022). Blue and greenwater footprint of agro-industrial avocado production in central Mexico. *Sustainability, 14*, 9664. https://doi.org/10.3390/su14159664

Gupta, S., & Jain, A. K. (2021). Biosorption of Ni (II) from aqueous solutions and real industrial wastewater using modified A barbadensis Miller leaves residue powder in a lab scale continuous fixed bed column Cleaner. *Cleaner Engineering and Technology, 5*, 100349. https://doi.org/10.1016/j.clet.2021.100349

GVR-4–68039–929–5., M. A. R. (2022). *Avocado Market Size, Share & Trends Analysis Report and Segment Forecasts, 2022 – 2030*

Ibrahim, F. M., Najeeb, D. A., & ThamerSadeq, H. (2023). Green preparation of Cu nanoparticles of the avocado seed extract as an adsorbent surface. *Materials Science for Energy Technologies, 6*, 130–136. https://doi.org/10.1016/j.mset.2022.12.006

Inyinbor, A. A., Adekola, F. A., & Olatunji, G. A. (2015). Adsorption of rhodamine b dye from aqueous solution on Irvingia gabonensis biomass: kinetics and thermodynamics studies. *South African Journal of Chemistry, 68*, 115–125. https://doi.org/10.17159/0379-4350/2015/v68a17

Ishikawa, M., Oaki, Y., Tanaka, Y., Kakisawa, H., Salazar-Alvarez, H., & Imai, H. (2015). Fabrication of nanocellulose–hydroxyapatite composites and their application as water-resistant transparent coatings. *Journal of Materials Chemistry, 3*, 5858. https://doi.org/10.1039/c5tb00927h

Kasiri, M. B. (2019). Application of chitosan derivatives as promising adsorbents for treatment of textile wastewater. In *The Impact and Prospects of Green Chemistry for Textile Technology* (pp. 417–469). The Textile Institute Book Series

Khamparia, S., & Jaspal, D. (2016). Investigation of adsorption of rhodamine B onto a natural adsorbent Argemone mexicana. *Journal of Environmental Management, 183*, 786–793. https://doi.org/10.1016/j.jenvman.2016.09.036

Lan, G., Qiu, Y., Fan, J., Wang, X., Tang, H., Han, W., Liu, H., Liu, H., Song, S., & Li, Y. (2019). Defective graphene@ diamond hybrid nanocarbon material as an effective and stable metal-free catalyst for acetylene hydrochlorination. *Chemical Communications, 55*, 1430–1433. https://doi.org/10.1039/c8cc09361j

Leite, A. J. B., Carmalin, S. A., Thuea, P. S., dos Reisa, G. S., Dias, S. L. P., Lima, E. C., Vaghettia, J. C. P., Pavan, F. A., & de Alencar, W. S. (2017). Activated carbon from avocado seeds for the removal of phenolic compounds from aqueous solutions. *Desalination and Water Treatment, 71*, 168–181. https://doi.org/10.5004/dwt.2017.20540

Ligas, B., Warchol, J., Skrzypczak, D., Witek-Krowiak, A., & Chojnacka, K. (2022). Valorization of biomass residues by biosorption of microelements in a closed-loop cycle. *Waste and Biomass Valorization, 13*, 1913–1929. https://doi.org/10.1007/s12649-021-01639-z

Lima, J. P., Alvarenga, G., Goszczynski, A. C. F., Rosa, G. R., & Lopes, T. J. (2020). Batch adsorption of methylene blue dye using Enterolobium contortisiliquum as bioadsorbent: Experimental, mathematical modeling and simulation. *Journal of Industrial and Engineering Chemistry, 91*, 362–371. https://doi.org/10.1016/j.jiec.2020.08.029

Liu, Q.-X., Zhou, Y.-R., Wang, M., Zhang, Q., Ji, T., Chen, T.-Y., & Yu, D.-C. (2019). Adsorption of methylene blue from aqueous solution onto viscose-based activated carbon fiber felts: Kinetics and equilibrium studies. *Adsorp. Sci. Technol., 37*, 312–332. https://doi.org/10.1177/0263617419827437

Liu, Z., Huang, X., Miao, Y., Gao, B., Shi, Y., Zhao, J., & Tan, S. H. (2022). Eggplant biomass based porous carbon for fast and efficient dye adsorption from wastewater. *Industrial Crops and Products, 187*, 115510. https://doi.org/10.1016/j.indcrop.2022.115510

Mahmoud, M. E., El-Said, G. F., Ibrahim, G. A. A., & Elnashar, A. A. S. (2022). Effective removal of hexavalent chromium from water by sustainable nano-scaled waste avocado seeds: Adsorption isotherm, thermodynamics, kinetics, and error function. *Biomass Conversion and Biorefinery*. https://doi.org/10.1007/s13399-022-03619-2

Mallampati, R., Xuanjun, L., Adin, A., & Valiyaveettil, S. (2015). Fruit peels as efficient renewable adsorbents for removal of dissolved heavy metals and dyes from water. *ACS Sustainable Chemistry & Engineering, 3*, 1117–1124. https://doi.org/10.1021/acssuschemeng.5b00207

Mokhtari, A., Sabzi, M., & Azimi, H. (2021). 3D porous bio-adsorbents based on chitosan/alginate/cellulose nanofibers as efficient and recyclable adsorbents of anionic dye. *Carbohydrate Polymers, 265*, 118075. https://doi.org/10.1016/j.carbpol.2021.118075

Naderir, M. (2015). Surface area: Brunauer–Emmett–Teller (BET). In *Progress in Filtration and Separation* (pp. 585–608). Academic Press.

Netto, M. S., da Silva, N. F., Stoffels Mallmann, E., Dotto, G. L., & Foletto, E. L. (2019). Effect of salinity on the adsorption behavior of methylene blue onto comminuted raw avocado residue: CCD-RSM design. *Water, Air, and Soil Pollution, 230*, 187. https://doi.org/10.1007/s11270-019-4230-x

Ortiz-Rodríguez, N. M., Condorí, M., Durán, G., & García-Valladares, O. (2022). Solar drying Technologies: A review and future research directions with a focus on agroindustrial applications in medium and large scale. *Applied Thermal Engineering, 215*, 118993. https://doi.org/10.1016/j.applthermaleng.2022.118993

Paniagua, S., Reyes, S., Lima, F., Pilipenko, N., & Calvo, L. F. (2021). Combustion of avocado crop residues: Effect of crop variety and nature of nutrients. *Fuel, 291*, 119660. https://doi.org/10.1016/j.fuel.2020.11966

Pereira, J. E. S., Ferreira, R. L. S., Nascimento, P. F. P., Silva, A. J. F., Padilha, C. E. A., & Barros Neto, E. L. (2021). Valorization of carnauba straw and cashew leaf as bioadsorbents to remove copper (II) ions from aqueous solution. *Environmental Technology and Innovation, 23*, 101706. https://doi.org/10.1016/j.eti.2021.101706

Permal, R., Chia, T., Arena, G., Fleming, C., Chen, J., Chen, T., Chang, W. L., Seale, B., Hamid, N., & Kam, R. (2023). Converting avocado seeds into a ready to eat snack and analysing for persin and amygdalin. *Food Chemistry, 399*, 134011. https://doi.org/10.1016/j.foodchem.2022.134011

Piedrahita-Rodríguez, S., Cardona Urrea, S., Escobar García, D. A., Ortiz-Sánchez, M., Solarte-Toro, J. C., & Cardona Alzate, C. A. (2023). Life cycle assessment and potential geolocation of a multi-feedstock biorefinery: Integration of the avocado and plantain value chains in rural zones. *Bioresource Technology Reports, 21*, 101318. https://doi.org/10.1016/j.biteb.2022.101318

Rahim, A. R. A., Mohsin, H. M., Chin, K. B. L., Johari, K., & Saman, N. (2021). Promising low-cost adsorbent from desiccated coconut waste for removal of Congo red dye from aqueous solution. *Water, Air, and Soil Pollution, 232*(9). https://doi.org/10.1007/s11270-021-05308-8

Rashama, C., Ijoma, G. N., & Matambo, T. S. (2022). Elucidating biodegradation kinetics and biomethane potential trends in substrates containing high levels of

phytochemicals: The case of avocado oil processing by-products. *Waste and Biomass Valorization, 13*, 2071–2081. https://doi.org/10.1007/s12649-021-01663-z

Rashid, R., Shafiq, I., Akhter, P., Iqbal, M. J., & Hussai, M. (2021). A state-of-the-art review on wastewater treatment techniques: The effectiveness of adsorption method. *Environmental Science and Pollution Research, 28*, 9050–9906. https://doi.org/10.1007/s11356-021-12395-x

Restrepo-Serna, D. L., Solarte-Toro, J. C., & Cardona-Alzate, C. A. (2022). A biorefinery approach for an integral valorisation of avocado peel and seeds through supercritical fluids. *Waste and Biomass Valorization, 13*, 3973–3988. https://doi.org/10.1007/s12649-022-01829-3

Rodríguez-Martínez, B., Romaní, A., Eibes, G., Garrote, G., Gullón, B., & del Río, P. G. (2022). Potential and prospects for utilization of avocado by-products in integrated biorefineries. *Bioresource Technology, 364*, 128034. https://doi.org/10.1016/j.biortech.2022.128034

Rotta, M., Rodrigues-Morais, D., Franca-Bionda, P., dos Santos, V., Matsushita, M., & Vergilio-Visentainer, J. (2016). Use of avocado peel (Persea americana) in tea formulation: A functional product containing phenolic compounds with antioxidant activity. *Acta Scientiarum Technology, 38*, 23–29. https://doi.org/10.4025/actascitechnol.v38i1.27397

Sahu, O., & Singh, N. (2019). Significance of bioadsorption process on textile industry wastewater. In *The Impact and Prospects of Green Chemistry for Textile Technology* (pp. 367–416). The Textile Institute Book Series.

San José, M. J., Álvarez, S., & López, R. (2023). Conical spouted bed combustor to obtain clean energy from avocado waste. *Fuel Processing Technology, 239*, 107543. https://doi.org/10.1016/j.fuproc.2022.107543

Sangaré, D., Moscosa-Santillan, M., Aragón Piña, A., Bostyn, S., Belandria, V., & Gokalp, I. (2022). Hydrothermal carbonization of biomass: Experimental study, energy balance, process simulation, design, and techno-economic analysis. *Biomass Conversion and Biorefinery*. https://doi.org/10.1007/s13399-022-02484-3

Shahbandeh, M. (2022). *Global avocado production 2000–2020*

Souza, F. H. M., Leme, V. F. C., Costa, G. O. B., Castro, K. C., Giraldi, T. R., & Andrade, G. S. S. (2020). Biosorption of rhodamine B using a low-cost biosorbent prepared from inactivated Aspergillus oryzae cells: Kinetic, equilibrium and thermodynamic studies. *Water, Air, and Soil Pollution*, *231*(5). https://doi.org/10.1007/s11270-020-04633-8

Tesfaye, T., Ayele, M., Gibril, M., Ferede, E., Limeneh, D. Y., & Kong, F. (2022). Beneficiation of avocado processing industry by-product: A review on future prospect. *Current Opinion in Environment Sustainability, 5*, 100253. https://doi.org/10.1016/j.crgsc.2021.100253

Venugopal, V. (2022). Green processing of seafood waste biomass towards blue economy. *Current Opinion in Environment Sustainability, 4*, 100164. https://doi.org/10.1016/j.crsust.2022.100164

Villaescusa, I., Fiol, N., Poch, J., Bianchi, A., & Bazzicalupi, C. (2011). Mechanism of paracetamol removal by vegetable wastes: The contribution of π-π interactions, hydrogen bonding and hydrophobic effect. *Desalination, 270*, 135–142. https://doi.org/10.1016/j.desal.2010.11.037

Wang, L., Shi, C., Wang, L., Pan, L., Zhang, X., & Zou, J. (2020). Rational design, synthesis, adsorption principles and applications of metal oxide adsorbents: A review. *Nanoscale, 12*, 4790–4815. https://doi.org/10.1039/C9NR09274A

Xing, W., Ngo, H. H., Kim, S. H., Guo, W. S., & Hagare, P. (2008). Adsorption and bioadsorption of granular activated carbon (GAC) for dissolved organic carbon (DOC) removal in wastewater. *Bioresource Technology, 99*, 8674–8678. https://doi.org/10.1016/j.biortech.2008.04.012

Yadav, A., Bagotia, N., Yadav, S., Sharma, N., Sharma, A. K., & Kumar, S. (2022). Environmental application of Saccharum munja biomass-derived hybrid composite for the simultaneous removal of cationic and anionic dyes and remediation of dye polluted water: A step towards pilot-scale studies. *Colloids and Surfaces a: Physicochemical and Engineering Aspects, 650*, 129539. https://doi.org/10.1016/j.colsurfa.2022.129539

Yu, J.-G., Yue, B.-Y., Wu, X.-W., Liu, Q., Jiao, F.-P., Jiao, X.-Y., & Chen, X.-Q. (2016). Removal of mercury by adsorption: A review. *Environmental Science and Pollution Research, 23*, 5056–5076. https://doi.org/10.1007/s11356-015-5880-x

Zafar, T., & Sidhu, J. S. (2011). Avocado: Production, quality, and major processed products. In N. K. Sinha, *Handbook of Vegetables and Vegetable Processing* (pp. 525–543)

Zhang, H., Wu, C., Li, Z., Su, Y., & Peng, B. (2023). Adsorption effects and regeneration characteristics of heavy bio-oil template porous carbon on Congo red. *Biomass Conversion and Biorefinery, 3*, 1–9. https://doi.org/10.1007/s13399-023-04131-x

Zimnitsky, D. S., Yurkshtovich, T. L., & Bychkovsky, P. M. (2006). Adsorption of zwitterionic drugs onto oxidized cellulose. *Journal of Colloid and Interface Science, 295*, 33–40. https://doi.org/10.1016/j.jcis.2005.07.058